PhD Dissertation

Bálint Szabó

2003

Probing Cellular Dynamics:
Fluctuations and Organized Motility

Bálint Szabó

Supervisors: Noémi Rozlosnik, PhD, Associate Professor and Prof. Tamás Vicsek, member of the Hungarian Academy of Sciences

Department of Biological Physics

Program for Statistical Physics, Biological Physics, and Quantum Systems
Head of Program: Tamás Vicsek

Graduate School of Physics,
Head of School: Prof. Zalán Horváth

Eötvös University, Budapest

Preface

Variety is the soul of pleasure

During my PhD studies I have worked with people from diverse backrounds: physics, biology, chemistry and medicine. This thesis is an outcome of such interdisciplinary co-operation. The power of physics applied to the colorful variety of biological phenomena is growing into a vivid branch of science. I hope that this work can be an expansion of biological physics.

Contents

Chapter 1

Introduction

1.1 Motion on the cellular level: between random and organized

Keep you moving

It is not only the muscle cells that can exert force and make movement. Cells need to move actively in numerous biological processes. For example, during embryonic development, each cell moves towards its destination. After an injury of a tissue, similar guided motility can be observed when destroyed cells are replaced. Leukocytes make their ways to the location of inflammation. Tumor cells making metastasis can invade into dense tissues and pass through the walls of blood-vessels.

Motility of animal cells is driven by motor proteins and fibrous protein polymers of the cytoskeleton. Changes in the nanoscale conformation of the motor proteins or the polymerization-depolymerization of cytoskeletal fibers lead to cellular motility. Biochemical reactions in the background of molecular dynamics need fluctuations (reasonable temperature) to work. On the scale of molecules (even huge macromolecules and polymers such as DNA) animals seem to be stochastic systems with random motion dominated by fluctuations. However, the motion of animals can be extremely well organized and controlled precisely. Cells in culture lie on the border between random and organized motility. We tried to shed light on some features of cellular dynamics down to the nanoscale in order to get closer to the link between random and organized motion [78].

The motility of animal cells is dominated by actin-myosin-based contraction and actin polymerization-based protrusion. The two basic types of protrusions, lamellipodia and filopodia are driven by actin polymerization-depolymerization processes [47, 16, 12]. Although statistical physics [49, 60] provides theory to explain such biological motilities, it is still on an elementary level and therefore needs to be developed.

1.2 Cytoskeleton

(The skeleton of this section is based on [2], Chapter 16 and further review articles. Consequently, most figures originate from these sources. In a few cases exact quotations are presented. The origin of the figures or quotations is indicated in the caption or in the text in italics.)

The cytoplasm of the eukaryotic cells is highly organized by filamentous structures such as fibrous actin (F-actin), microtubules (MT-s) and intermediate filaments (IF-s). Actin and MT-s have been extensively investigated in the past decades but less is known about IF-s. These 3 major types of protein fibers together with the numerous associated proteins make a network called cytoskeleton. The elasticity of cells is mainly determined by the dynamic system of the cytoskeleton. MT-s are very stiff hollow tubes with persistence lengths of millimeters. The more flexible F-actin usually builds up bundles -joined by actin binding proteins- or cross-linked aggregates. IF-s are relatively tough fibers, known to give mechanical stability to cells ([2], chapter 16).

1.2.1 Microtubules

MT-s polymerize from tubulin dimers (one α- with one β-tubulin monomer). They are located throughout the cytoplasm governing the location of many cell components. A MT is built up from 13 linear protofilaments forming a cylinder. Each protofilament is a chain of alternating α- and β-tubulin subunits (Fig. 1.2.1).

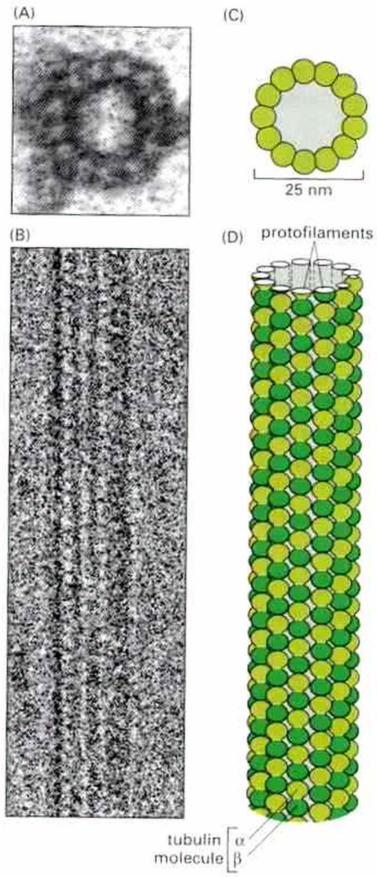

Figure 1.1: (A) Electron micrograph of a microtubule seen in cross section, with its ring of 13 distinct subunits, each of which corresponds to a separate tubulin molecule (an α/β heterodimer). (B) Cryoelectron micrograph of a microtubule assembled *in vitro*. (C and D) Schematic diagrams of a microtubule, showing how the tubulin molecules pack together to form the cylindrical wall. (C) The 13 molecules in cross-section. (D) A side view of a short section of a microtubule, with the tubulin molecules aligned into long parallel rows, or *protofilaments*. Each of the 13 protofilaments is composed of a series of tubulin molecules, each an α/β heterodimer. Note that a microtubule is a polar structure, with a different end of the tubulin molecule (α or β) facing each end of the microtubule. *(Source: [2], p. 803.)*

Protofilaments are aligned with the same polarity, which infers that MT-s are polar structures with a so called + (fast growing) and - (slow growing) end. MT-s are dynamic structures. In a typical fibroblast cell 50% of the tubulin is free and the other 50% is in MT-s. In the presence of GTP and Mg^{2+} tubulin polymerize into MT-s. The elongation of the tubes is much faster than their nucleation. The rate of dimer association to the + end is higher than to the - end. Even when the length of MT-s is constant, monomers may be associating to the + end and dissociating from the - end of the polymer. This is the phenomenon of treadmilling. MT dynamics runs on the minute time scale.

Individual MT-s grow in cells at a constant rate for a while, then shrink abruptly toward the centrosome. This behavior is called dynamic instability. Both α and β tubulin bind GTP. In a MT the β subunit hydrolyzes its bound GTP, which has relevance in the dynamic behavior of MT-s. GTP binding is required for MT polymerization, while hydrolysis is not. MT growth is usually faster than GTP hydrolysis, which results

in the formation of a so called GTP cap at the + end (Fig. 1.2).

Probably the delayed GTP hydrolysis after tubulin assembly causes the dynamic instability. GTP cap stabilizes the + end, since tubulin molecules with GTP bind to each other with higher affinity. The loss of the GTP cap facilitates the disassembly of the MT.

In most interphase animal cells, MT-s grow out of the centrosome. (But in oocytes, for instance, there is no centrosome.) The centrosome, which contains 2 centrioles positioned at right angles to each other, is usually located close to the nucleus. Centrioles are cylindrical structures; their wall is constituted by 9 groups of MT triplets. See Fig. 1.2.1. Surrounding the centrioles a network of small fibers can be observed: the centrosome matrix, which nucleates MT polymerization. Although the exact structure and the MT nucleating mechanism of the centrosome is unknown, it is known that a third type of tubulins, γ-tubulin, is present in it. γ-tubulin forms rings and spirals in the centrosome made of 13 tubulin monomers. These are involved in the nucleation of MT-s. The so-called ring complex contains a ring of 13 γ-tubulin molecules and other associated proteins. However, ring complexes can be found outside the centrosome, these do not nucleate MT polymerization.

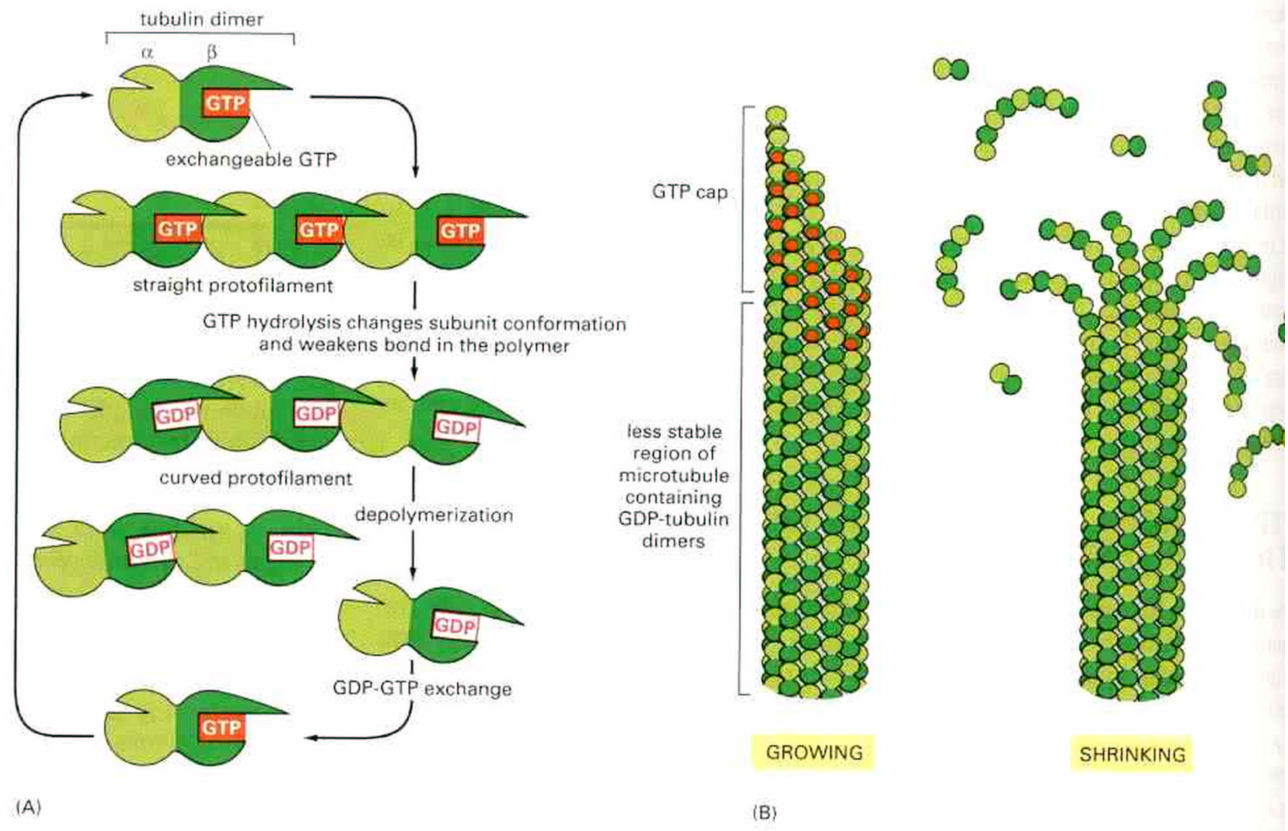

Figure 1.2: (A) Addition of tubulin heterodimers carrying GTP to the end of a protofilament causes it to grow in a linear conformation that can readily pack into the cylindrical wall of the microtubule, thereby becoming stabilized. Hydrolysis of GTP after assembly changes the conformation of the subunits and tends to force the protofilament into a curved shape that is less able to pack into the microtubule wall. (B) In an intact microtubule protofilaments made from GDP-containing subunits are forced into a linear conformation by the many lateral bonds within the microtubule wall, especially in the stable cap of GTP-containing subunits. Loss of the GTP cap, however, allows the GDP-containing protofilaments to relax to their more curved conformation. This leads to progressive disruption of the microtubule and the eventual disassembly of protofilaments into free tubulin dimers. *(Source: [2], p. 810)*

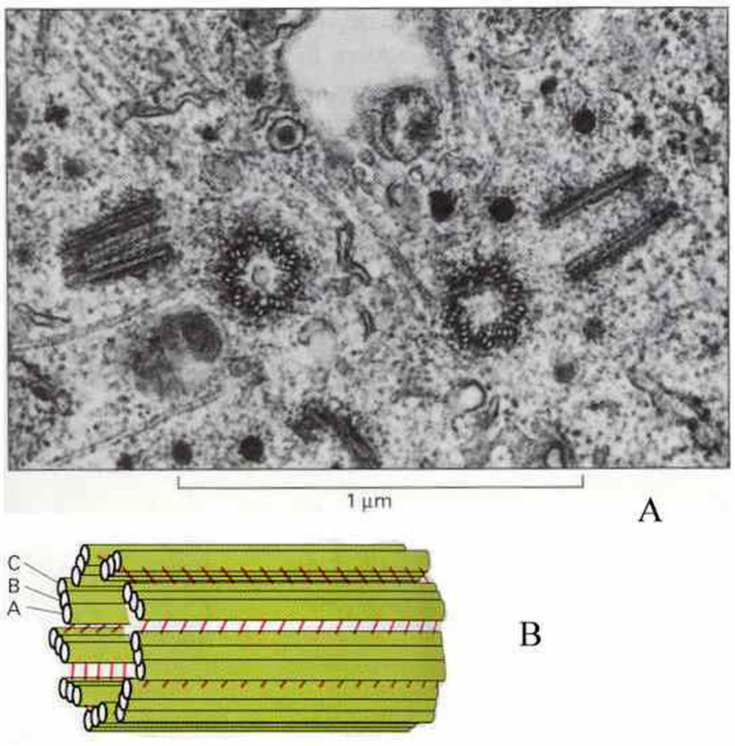

Figure 1.3: (A) An electron micrograph showing a newly replicated pair of centrioles. One centriole of each pair has been cut in cross-section and the other in longitudinal section, indicating that the two members of each pair are aligned at right angles to each other. (B) Schematic diagram of a centriole viewed from the side. *(Source: [2], p. 818. and 819.)*

The intracellular transport of cellular organelles is mainly mediated by MT motors. Proteins from the 9 kinesin and 3 dynein families are MT associated motors that can walk along MT-s while carrying cargos or make slide antiparallel MT-s over each other. Cytoplasmic dyneins are involved in the mitosis and the transport of organelles. Kinesins transport organelles and synaptic vesicles, and take part in mitosis and meiosis. Both kinesins and dyneins are ATPase motors, composed of 2 heavy chains and several light chains moving in only one direction along MT-s: either + end or - end motors. Heavy chains contain a globular ATP binding head and a tail of rodlike domains: Fig. 1.4. The head binds the MT and the cargo can attach to the tail. Most kinesins are + end motors, all dyneins walk towards the - end. The MT binding and ATPase affinity is probably modified by the attachment of the cargo via the interaction of the head and tail regions. The tail is thought to be cargo specific: the motor domain in the head is highly conserved among different kinesins but the stalk and tail are variable (Fig. 1.5). Stalk domains serve for the dimerization of kinesins. 3 types of kinesins are known: N-kinesins (conventional kinesins) are generally + end motors with a motor domain on the N (amino) terminal of the polypeptides, C-kinesins having C terminal motor domains are - end motors, I-kinesins are not real motors but MT destabilizing factors. The directionality of kinesins is thought to be determined by the neck region. Dyneins are protein giants as compared to kinesins. They are much faster, as well. Kinesins are processive motors: they can walk along an MT without dissociating from it for several hundred steps. Dyneins are not processive.

Posttranslational modifications of tubulin after polymerization provide information of the age of the MT. The slow acetylation and detyrosination of α-tubulin occurs only on tubulin molecules of MT-s. Free tubulin will be reversed soon after depolymerization. Both extremely stable and labile MT-s can be found. Not only centsosome but microtubule associated proteins (MAP-s) control the

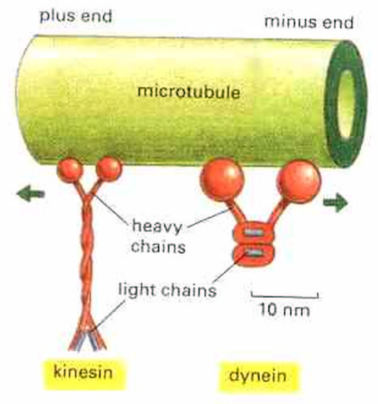

Figure 1.4: Microtubule motor proteins. Kinesins and cytoplasmic dyneins are microtubule motor proteins that generally move in opposite directions along a microtubule. These proteins (drawn here to scale) are complexes composed of two identical heavy chains plus several smaller light chains. Each heavy chain forms a globular head region that attaches the protein to microtubules in an ATP-dependent fashion. *(Source: [2], p. 814.)*

dynamics of MT-s. A structure MAP can be either MT stabilizing or destabilizing protein. Some MAP-s bundle MT-s. Bundles are usually more stable. The outer wall of MT-s is negatively charged: numerous MT-binding molecules, including some MAP-s, are anchored to the MT-s by electrostatic interaction. The expression of MAP-s is highly tissue- and age-specific. Furthermore, even in a single neuron, different MAP-s are localized in different regions. (E.g. τ MAP bundles the axonal MT-s and MAP2 makes the bundling of the dendritic MT-s.)

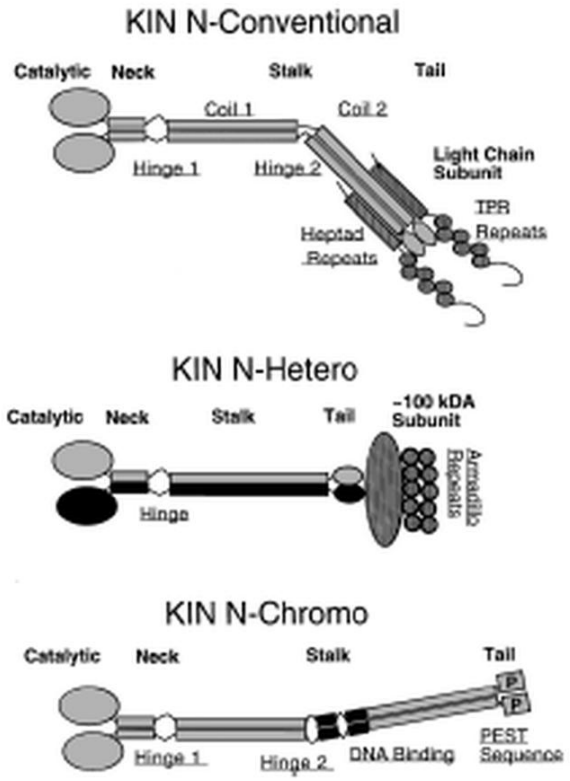

Figure 1.5: Architecture of kinesin motors. The overall structural features of three well-studied kinesin motors are shown here. The precise organization of the tail domains and how subunits interact with the tail domains are speculative at this time. Motor containing polypeptide chains are indicated (by gray or black area), and associated subunits are indicated by hatched area. The KIN N-Conventional and KIN N-Chromo motors are homodimers of two identical motor-containing polypeptides, whereas KIN N-Hetero motors are heterodimers of two non-identical subunits (indicated by the black and gray coloring). *(Source: [76])*

MAP2 binds other proteins such as calmodulin and A kinase: it can organize supramolecular complexes. MAP2 is reactive to proteolytic cleavage, which results in its fast turnover. The MAP2-MT system might be a source of synaptic plasticity. MAP-s inhibit axonal transport, since they disturb the walk of MT motors. Probably MAP-s dissociate from the MT when kinesin or dynein comes. The MT affinity of MAP-s can be regulated by phosphorylation. Some MAP-s, e.g. SCG10 induce the depolymerization of MT-s, katanin severs MT-s, and catastrophy factors will make the MT system fall apart abruptly.

1.2.2 Actin

All eucaryotic species have actin, an ATPase molecule. Two forms of actin can be observed in cells: globular actin (G-actin) and fibrous actin (F-actin). F-actin is about 8 nm wide and consist of a helix of G-actin molecules oriented in the same direction (Fig. 1.2.2), resulting in a polar structure with a fast growing + or 'barbed' and a slow growing - or 'pointed' end similarly to MT-s. (Nomenclature comes from the shape of myosin decoration of MT-s.)

The ATP- and cation-dependent actin polymerization is a basic engine of cellular motion. It drives locomotion (crawling) of cells and has a role in cellular shape formation. Actin dynamics with a characteristic time on the scale of seconds (much faster than MT dynamics) is controlled by a complex and sophisticated system. The nucleation of F-actin growth is slower than the elongation process just as in the case of MT-s. The nucleating structure is thought to be a trimer of actin molecules. The critical concentration of G-actin i.e., the concentration, at which the quantity of F-actin is constant, is lower than the actual G-actin concentration in the cells. It means that certain mechanisms can retain G-actin from polymerization. After the assembly of an actin molecule into the fiber, ATP gets hydrolysed, which is analogous to the GTP cleavage in an MT. The clam-shaped actin molecule binds ATP between the 2 halves of the clam that can open and close. Intermolecular interactions between actin monomers in the fiber close the shell. The cleavage of ATP is considered to be initiated by the closure of the

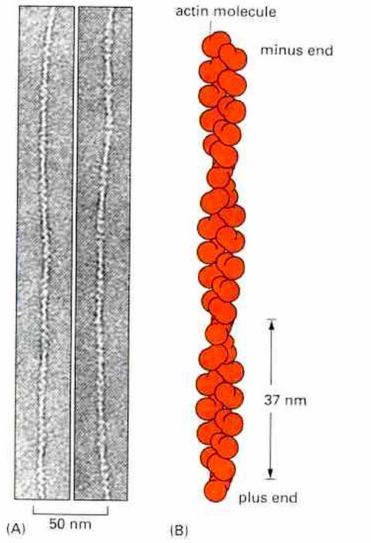

Figure 1.6: Actin filaments. (A) Electron micrographs of negatively stained actin filaments. (B) The helical arrangement of actin molecules in an actin filament. *(Source: [2], p. 821.)*

clam, soon after inorganic phosphate dissociates, and ADP remains trapped in the shell of the actin molecule. The ATP-ase activity is not required in the polymerization process. It rather weakens the interaction between the monomers, which promotes depolymerization resulting in an unstable pointed-end. Although F-actin does not show the effect of dynamic instability, a characteristic phenomenon of MT-s: treadmilling can be observed in many cases.

The properties and function of actin based intracellular structures is dependent on a large variety of actin-binding proteins (Fig. 1.7). 'Actin can assemble into many structures and participates in a wide range of processes in eukaryotic cells. The diversity of actin filament forms is only made possible by the association of actin with actin-binding proteins. Some of these proteins facilitate organization of filaments into higher order structures while others have regulatory functions, affecting the dynamics of filament turnover and allowing remodelling of the actin cytoskeleton in response to appropriate signals.' *(Quoted from [3].)*

Profilin and β-thymosin are G-actin-binding proteins [16]. Their main role is considered to be the G-actin sequestering, which decreases the available amount of G-actin for polymerization. It enables cells to answer quickly to either an extracellular or an intracellular signal by switching on the actin polymerization, because large amounts of G-actin dissociate from β-thymosin or profilin, if their actin-binding affinity drops due to the signal. Although profilin inhibits F-actin nucleation, it stimulates the nucleotide exchange on actin molecules and promotes the elongation of the barbed-end. Proteins from the ADF/cofilin family (AC proteins) bind both G- and F-actin and destabilize F-actin. Cofilin binds predominantly close to the pointed-end where actin monomers have ADP inside causing the depolymerization of the pointed-end. Cofilin speeds up the turnover of actin and results in fast nett F-actin growth. Gelsolin after Ca^{2+} activation or AC proteins can sever the actin filaments generating more free ends for polymerization or depolymerization. While capping proteins and gelsolin cap the barbed-end to regulate the incorporation or dissociation of actin monomers, the members of the Arp protein family cap the pointed-end and nucleate filament growth.

Actin in the gel-like network of the cell cortex (perimeter of the cell beneath the plasma membrane) gives elasticity and mechanical stability to cells among other fibrous proteins, especially spectrin. Cell shape is predominantly determined by this actin-rich network. Further 2 types of arrays can be observed in the cortical actin structure of cells: parallel and contractile bundles.

The two well-known protrusive structures are the lamellipodium and filopodium in migrating cells. In lamellipodia, actin fibers are organized to form a fan-shaped network by the Arp2/3 complex (Fig. 1.8). Arp2/3 nucleates the formation of actin filaments on pre-existing filaments. The angle of branching is $\sim 70°$. In filopodia, actin filaments are bundled and aligned with the same polarity by the protein fimbrin and/or fascin constituting a hexagonal tight packing as seen in the cross-section of filopodia. This type of packing prevents Myosin-II from entering into the bundle. On the contrary, myosin-II fits into the stress fibers that are bundled by the protein α-actinin. These contractile bundles

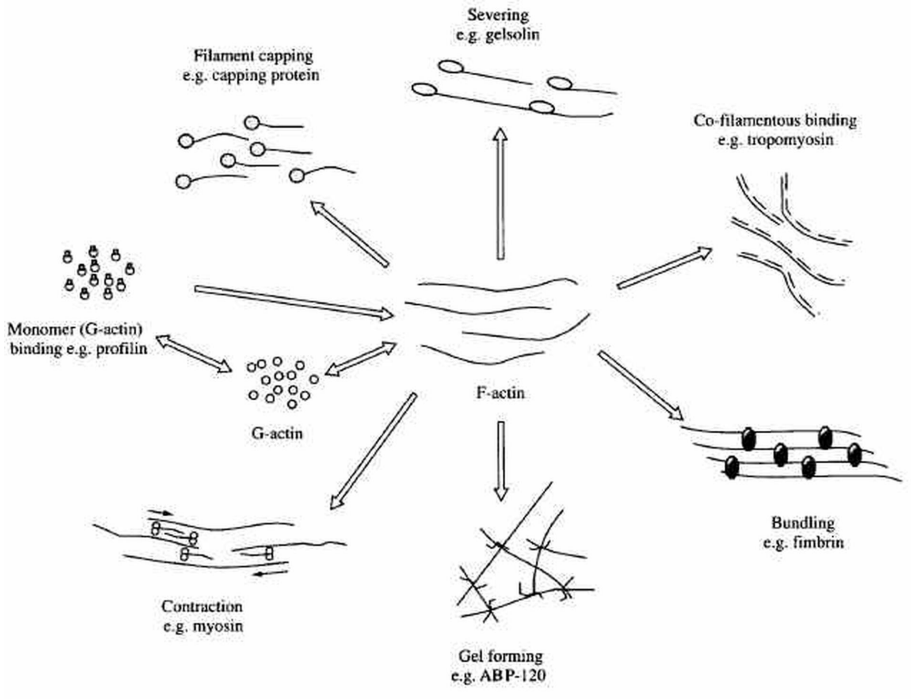

Figure 1.7: Functions of actin-binding proteins determined from *in vitro* research. Many actin-binding proteins have been purified and their properties and effects on actin have been extensively studied. How these in vitro functions relate to the role of the actin-binding proteins within a cellular environment remains largely unknown. Specific functions of actin-binding proteins are shown with a diagram of how each protein may interact with F-actin. Examples of proteins that may fulfil these functions are also given. *(Source: [3])*

are characteristic components of the fibroblast cytoskeleton resembling the myofibrils in muscle. They bridge between two focal contacts or a focal contact and intermediate filaments. Focal contacts are junctions between the intracellular actin filaments and the extracellular matrix mediated by integrins and a complex of proteins linking the end of F-actin and integrin (Fig. 1.18). Focal contacts take part in the signal transduction, too. Several protein kinases regulating proliferation and other domains of cell behavior are localized to focal contacts. Stress fibers keep tension across the cell; if cell contacts to the extracellular matrix disassemble, they will disappear. Stress fiber contraction is based on the slide of myosin-II fibers in relation to actin filaments, driven by the 'nodding' of myosin heads similarly to muscle contraction (Fig. 1.2.2).

Several myosin types can be observed in eucaryotic cells. Muscle myosin is from the myosin-II subfamily of myosins. They have two heads (motor domains with ATPase activity) and a rodlike tail. Two identical heavy chains, each complexed to a pair of light chains forms myosin-II (Fig. 1.9). The main function of the tail is to allow the molecules to polymerize into bipolar filaments. Even in non-muscle cells contractile bundles of actin and myosin-II are formed transiently, e.g., stress fibers. After completing their specific task they disassemble. The amount of myosin-I molecules in cells is far less. They have a conserved motor domain and further variable domains determining the specific role of the certain myosin (Fig. 1.10). Most myosins are + end motors but e.g., myosin VI walks toward the - end. The direction is determined by the core of the motor domain [40].

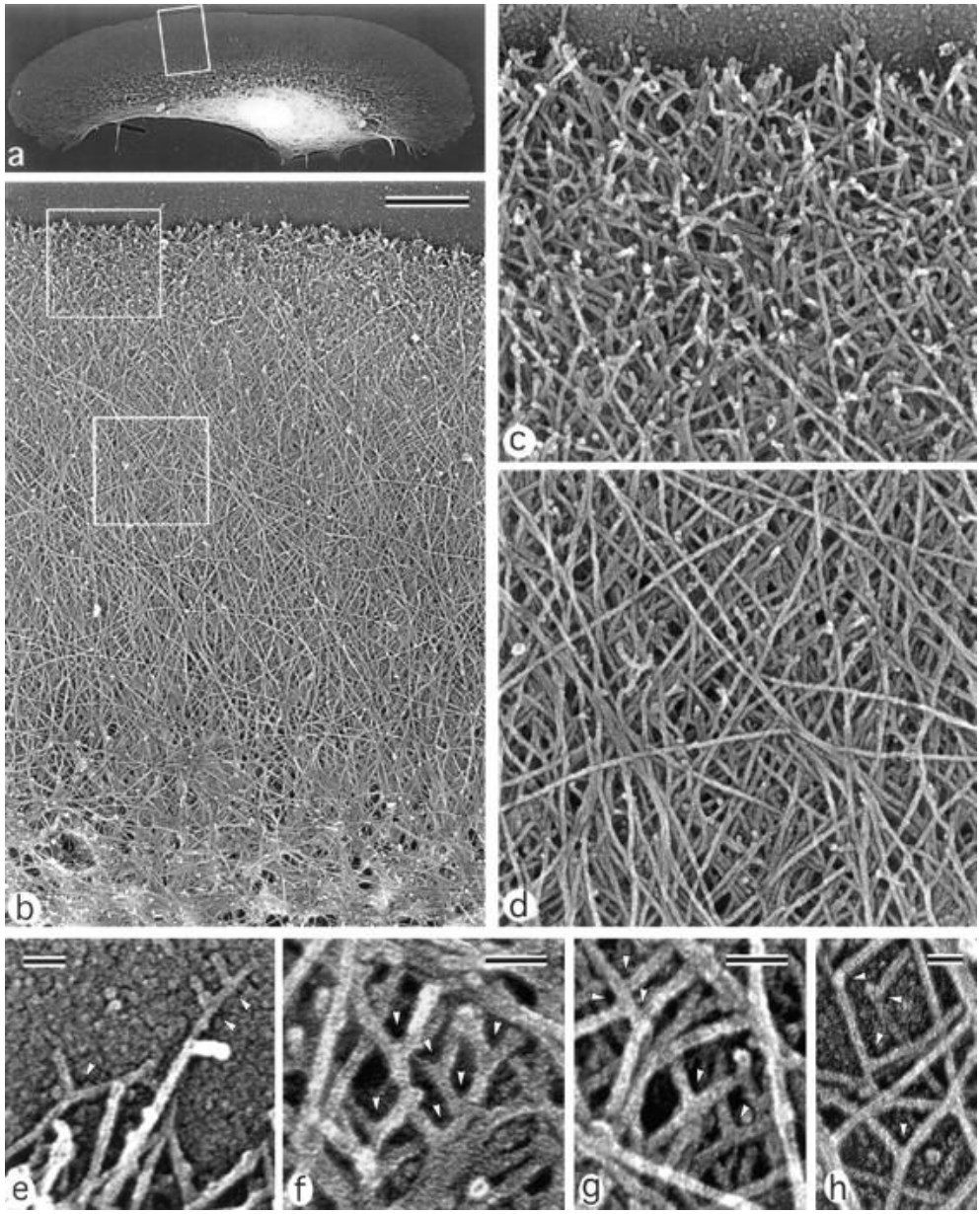

Figure 1.8: Organization of actin filaments in keratocyte lamellipodia. EM of detergent-extracted cells. (a) Overview of a locomoting cell; (b) actin network in lamellipodia from the leading edge (top) to the transitional zone (bottom); (c) brushlike zone at the leading edge with numerous filament ends; (d) smooth actin filament network in the middle part of lamellipodia; (e-h), T junctions (arrowheads) between filaments at the extreme leading edge (e), within the brushlike zone (f), in the central lamellipodia (g), and close to the lateral edge of the lamellipodia (h). The cell's leading edge is oriented upward in all panels. Boxed region in a is enlarged in b; upper and lower boxed regions in b are enlarged in c and d, respectively. Bars: (b) 1 μm; (e-h) 50 nm. *Source: [70].*

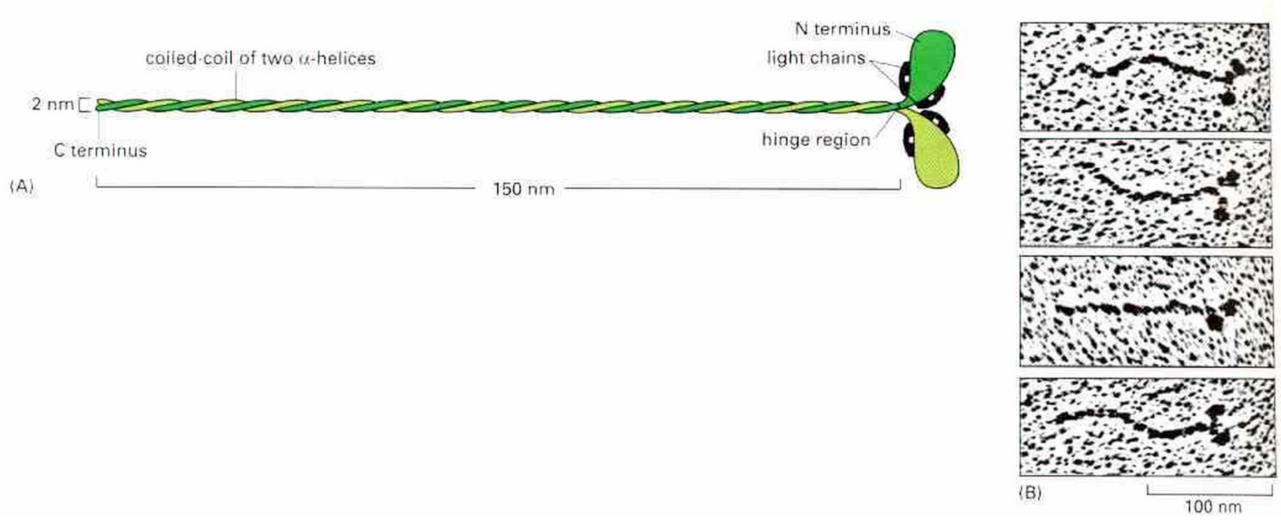

Figure 1.9: Myosin-II. (A) A myosin-II molecule is composed of two heavy chains (each about 2000 amino acids long) and four light chains. The light chains are of two types (one containing about 190 and the other about 170 amino acids), and one molecule of each type is present on each myosin head. Dimerization occurs by the two α helices wrapping around each other to form an α-helical coiled-coil, driven by the association of regularly spaced hydrophobic amino acids. The coiled coil arrangement makes an extended rod in solution, and this part of the molecule is termed the rod domain, or the tail. This type of structural motif is found in many other cytoskeletal proteins, enabling them to form an extended structure. (B) The two globular heads and the tail can be clearly seen in electron micrographs of myosin molecules shadowed with platinum. *(Source: [2], p. 838.)*

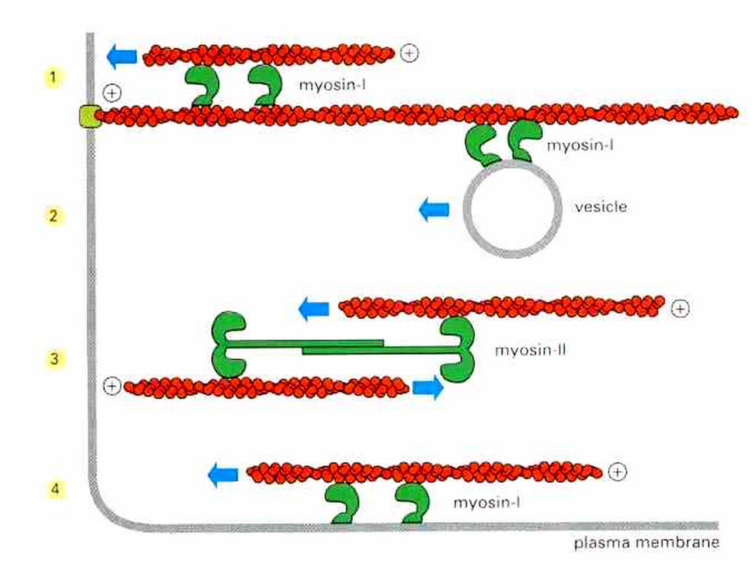

Figure 1.10: Possible roles of myosin-I and myosin-II in a typical eucaryotic cell. The short tail of a myosin-I molecule contains sites that bind either to other actin filaments or to membranes. This allows the head domain to move one actin filament relative to another (1), a vesicle relative to an actin filament (2), or an actin filament and membrane relative to each other (4). In addition, small antiparallel assemblies of myosin-II molecules can slide actin filaments over each other, thus mediating local contractions in an actin filament bundle (3). In all four cases the head group ”walks” toward the plus end of the actin filament it contacts. *(Source: [2], p. 839.)*

'Members of the Rho family of small Ras-like GTPases-including RhoA, -B, and -C, Rac1 and -2, and Cdc42-exhibit guanine nucleotide-binding activity and function as molecular switches, cycling between an inactive GDP-bound state and an active GTP-bound state. The Rho family GTPases participate in regulation of the actin cytoskeleton and cell adhesion through specific targets. Identification and characterization of these targets have begun to clarify how the Rho family GTPases act to regulate cytoskeletal structure and cell-cell and cell-substratum contacts in mammalian cells. The Rho family GTPases are also involved in regulation of smooth muscle contraction, cell morphology, cell motility, neurite retraction, and cytokinesis. However, the molecular mechanisms by which the Rho family GTPases participate in the regulation of such processes are not well established.' *(Quoted from [42].)* The GTP-bound form of proteins from the Rho family is active, whereas the GDP-bound state is inactive. Regulator and effector molecules interact with the Rho family members altering their GTPase activity (e.g., Rho GAP) or enhancing the exchange of the hydrolyzed nucleotide (e.g., Rho GEF) or influencing other properties related to the nucleotide-binding (Fig. 1.12). Extracellular ligands can activate GTPases from the Rho famyily. Bradykinin and TNFα stimulates Cdc42; PDGF, EGF, insulin, and bombesin activates Rac1; LPA and bombesin induces the stimulus of RhoA.

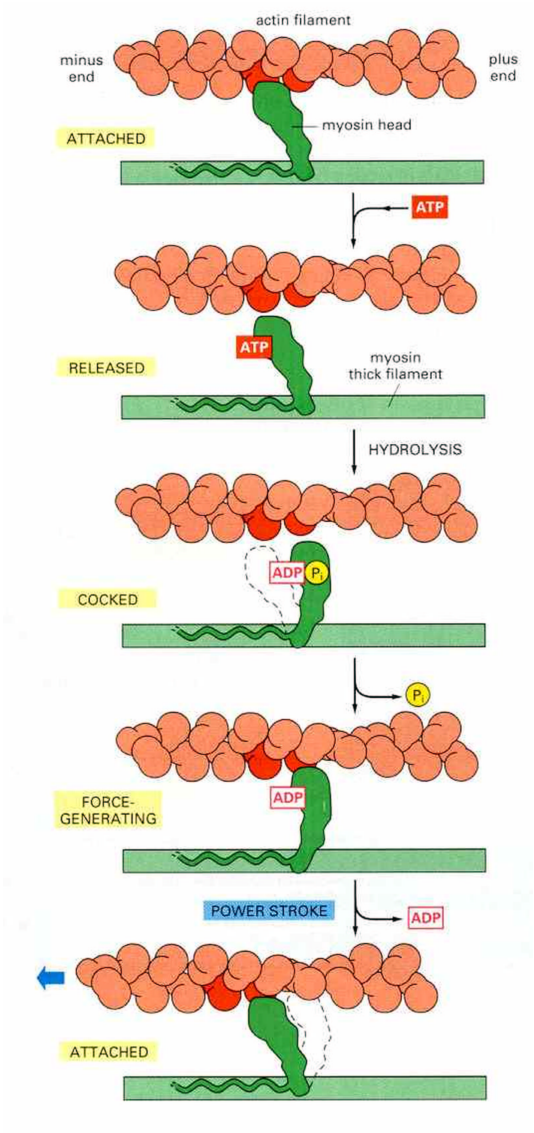

Figure 1.11: The cycle of changes by which a myosin molecule walks along an actin filament. *(Source: [2], p. 852.)*

Downstream signaling pathways mediated by the members of the Rho family are shown in Fig. 1.14 and Fig. 1.13. These are not separated pathways but they cross-talk between each other. (See e.g., [18].) Whereas, Rac and Cdc42 stimulates cell motility Rho induces the formation of stable stress fibers resulting in a rather stationary cellular behavior.

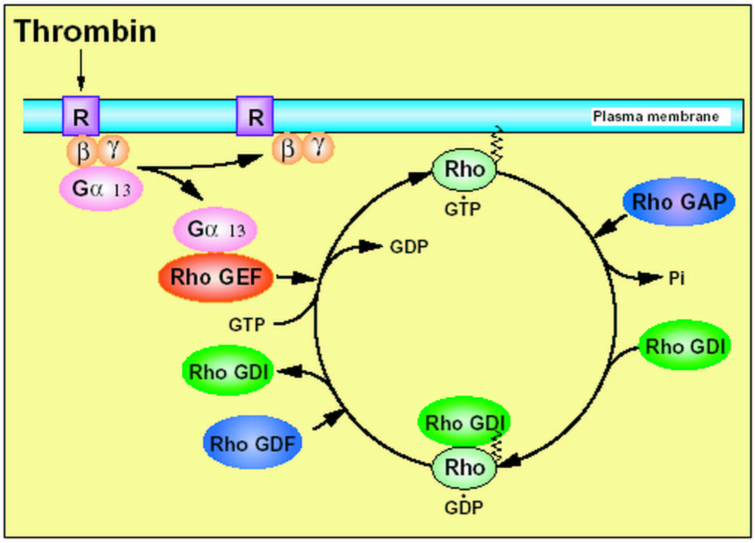

Figure 1.12: Mode of activation of the Rho family GTPases. Extracellular signal (e.g., the binding of the protein thrombin) to a trimeric G protein-linked seven-transmembrane receptor (R) induces the dissociation of the α subunit (Gα) from the β and γ subunits by the exchange of the bound GDP to GTP in the α subunit. The activated α subunit relays the signal to an effector (Rho GEF) of the Rho protein. GEF, Guanine nucleotide exchange factors; GAP, GTPase-activating proteins; GDI, GDP dissociation inhibitor; GDF, GDI dissociation factor. *Source: [42]*

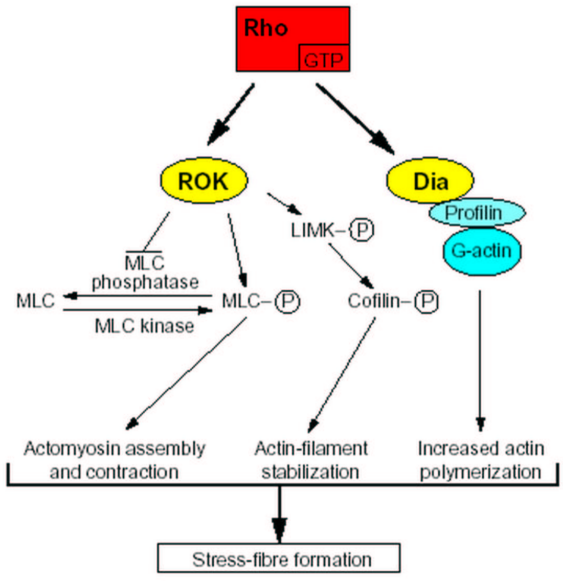

Figure 1.13: Signal-transduction pathways involved in Rho-induced stress-fibre assembly. *Source: [10]*

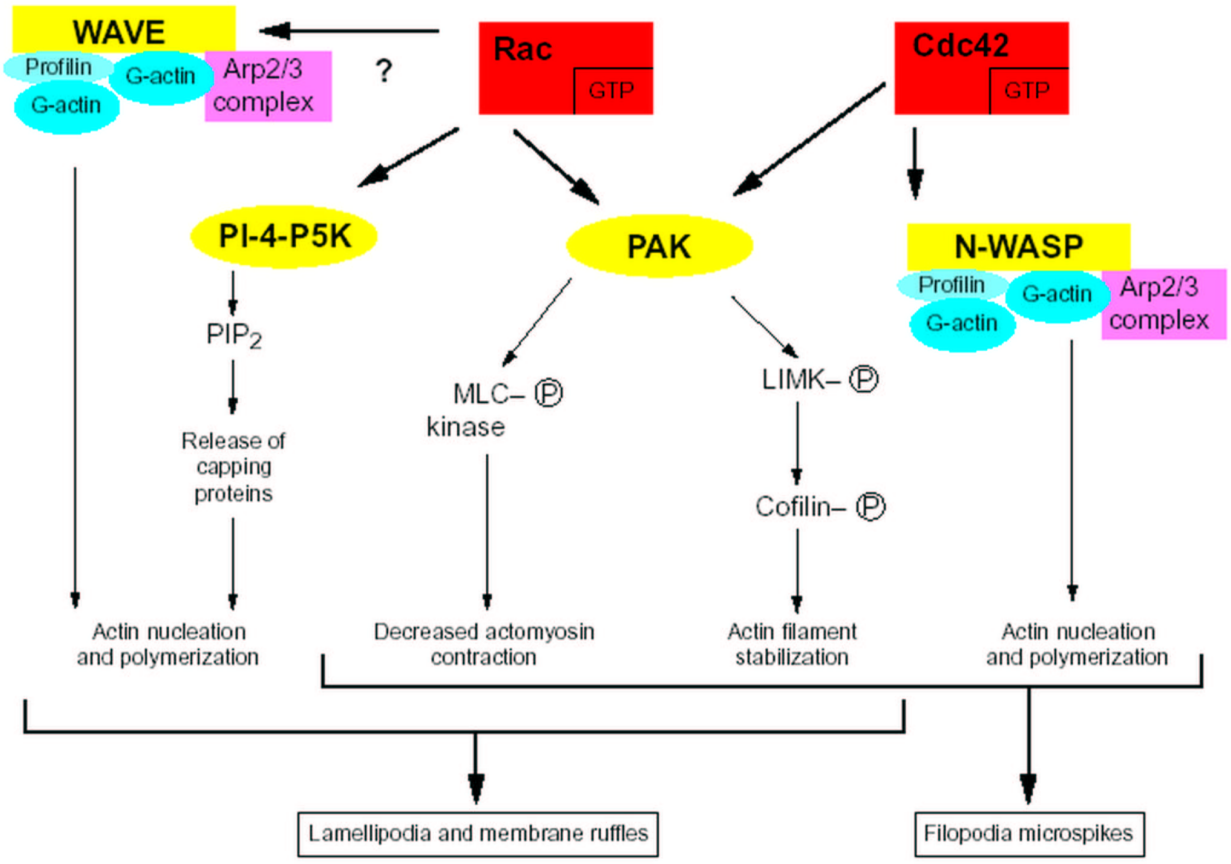

Figure 1.14: Signal-transduction pathways induced by Rac and Cdc42 (shown in red), which are thought to contribute to the formation of actin-containing lamellipodia and filopodia respectively. *Source: [10]*

1.2.3 Intermediate filaments

'Intermediate filaments are tough and durable protein fibers found in the cytoplasm of most, but not all, animal cells.' *(Quoted from [2], p. 796.)* The nucleus usually surrounded by a meshwork of IF-s, which extends to the plasma membrane. The nuclear envelope also underlaid by an IF network, the so called nuclear lamina. IF monomers are elongated fibrous proteins unlike actin and tubulin. IF polymers are nonpolarized, which distinguishes them from MT-s and F-actin (Fig. 1.15) [77].

1.3 Cell-extracellular matrix interactions

(The skeleton of this section is based on [2], Chapter 19.)

In animals the space between cells is mainly filled by the extracellular matrix (ECM), which is a meshwork of proteins and polysaccharides (Fig. 1.16). ECM is not only a scaffold for cells but rather an active medium that interacts with cells and influences their development, proliferation, motility, shape, and function. We used fibronectin, a large glycoprotein in our nuclear motility experiments as a cell adhesive agent. Type III fibronectin repeat is a characteristic module of fibronectin (Fig. 1.17). This module contains the Arg-Gly-Asp (RGD) sequence, which can bind to the integrin cell surface receptors.

Integrins are the transmembrane linker molecules between intracellular actin filaments and extracellular matrix proteins (FIG. 1.18 and Fig. 1.19). These molecular contacts also take part in signal transduction. Cells from the adherent type lacking cell-substrate contacts will not survive, which is a rather controlled behavior as a consequence of the missing signal.

1.4 Cell migration

Cell locomotion is driven by actin polymerization and actomyosin contractions. At the leading edge of the cell actin polymerization pushes the plasma membrane forward in the lamellipodium (Fig. 1.8. During the outgrowth of the lamellipodium the cell body with the nucleus usually stay fixed relative to the substrate due to the focal contacts and other cell-matrix junctions. Both the transport of the cell body to the leading edge and the consecutive retraction of the rear part of the cell -the tail- is known to be mediated by actomyosin contraction. In most cases the above mentioned 3 distinct steps are accepted to make up the cellular locomotion. Although, in the course of locomotion the nucleus is transported forward via an actomyosin based machinery, nuclear positioning and fast translocation of the nucleus is generally driven by an MT-dependent system, e.g., in budding yeast or in the oocyte of some animals.

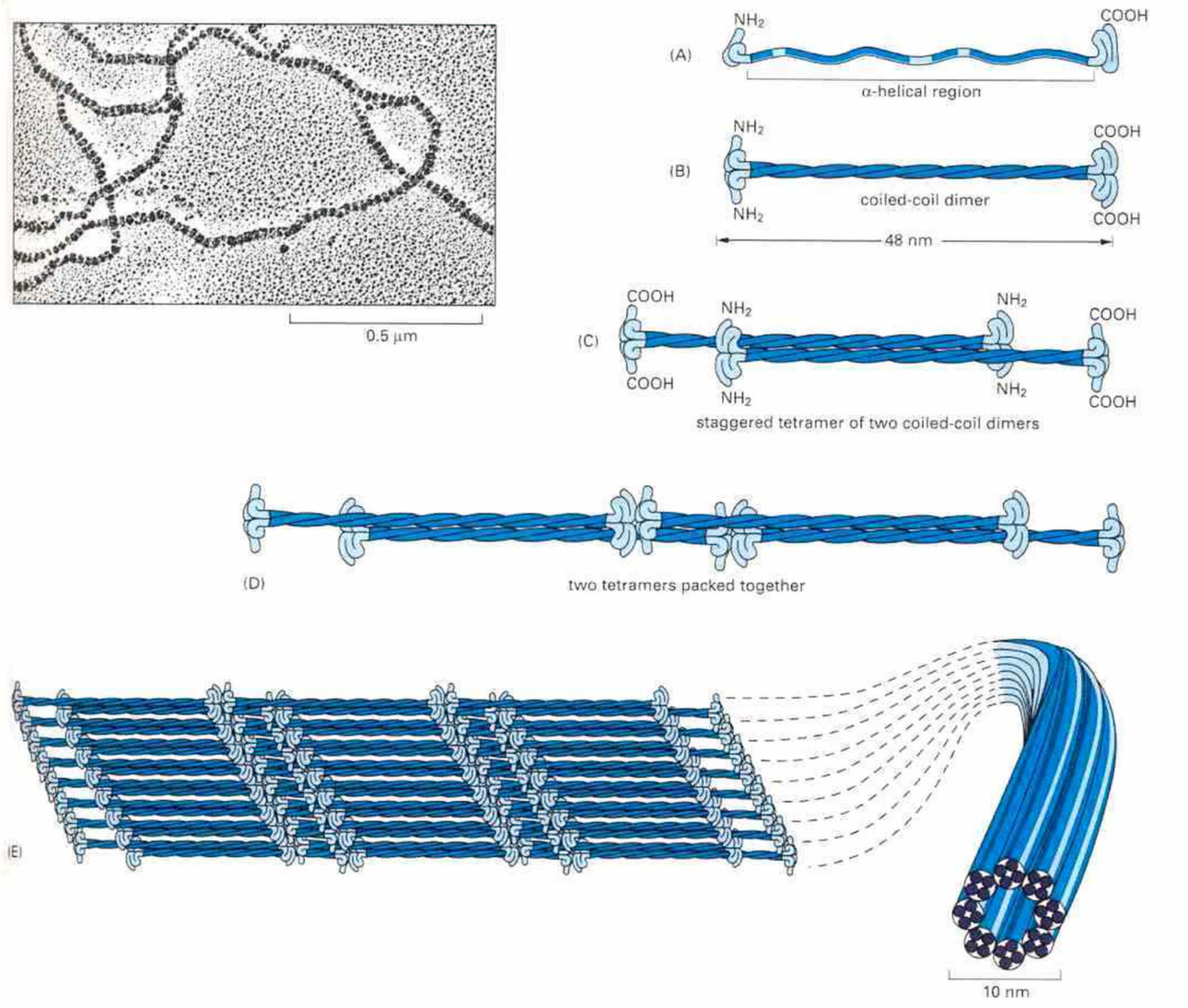

Figure 1.15: A current model of intermediate filament construction. The monomer shown in (A) pairs with an identical monomer to form a dimer (B) in which the conserved central rod domains are aligned in parallel and wound together into a coiled-coil. Two dimers then line up side by side to form an antiparallel tetramer of four polypeptide chains (C). Within each tetramer the dimers are staggered with respect to one another, thereby allowing it to associate with another tetramer, as shown in (D). In the final 10-nm intermediated filament, tetramers are packed together in a ropelike array (E). An electron micrograph of the final filament is shown upper left. *(Source: [2], p. 797.)*

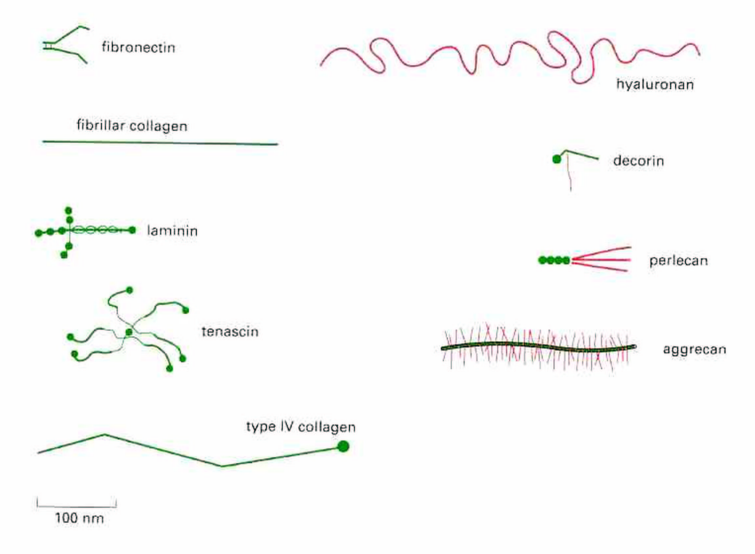

Figure 1.16: The comparative shapes and sizes of the major extracellular matrix macromolecules. Protein is shown in green, glycosaminoglycan in red. *(Source: [2], p. 992.)*

1.5 Nuclear motility

Intracellular transport of organelles can be basically actin- or MT-dependent. Both the polymerization of actin/MT-s and molecular motors can drive intracellular motility. Vesicles and more complex organelles with membrane boundary, such as endoplasmic reticulum, golgi apparatus, and the nucleus [63] are usually positioned, aligned and transported in the cell in an MT-dependent way. Although, kinesins and cytoplasmic dyneins are the main tools of this transport the positioning of the nucleus -e.g., in yeast- needs MT-polymerization. In mitosis, besides the action of several MT motors, organized MT-polymerization is also required to pull apart the chromosomes. Some bacteria can move with an enormous speed in cells using an actin-polymerization-driven engine: an actin comet tail pushes forward these parasites.

Migrating cells translocate their cell bodies to the leading edge by nucleokinesis [43]. This process is known to be critically MT-dependent [23]. In the developing brain distinct modes of neuronal migration are known [56]. In all modes the nucleus is translocated along the elongated neuron in a presumably MT-dependent way [52, 53]. In the ventricular zone (VZ) the nuclei of neuronal progenitor cells and radial glial cells oscillate between the borders of the VZ 1.20, which is known as interkinetic nuclear movement and has important role in the development of the brain [54]. This nuclear motility is coupled to the cell cycle. Lissencephaly (smooth brain) is a serious disease, in which the migration of neurons to the cerebral cortex is inhibited. The abnormally low level of the LIS1 protein causes lissencephaly. The similarity between LIS1 and NUDF -nuclear migration protein from *A. nidulans*: a worm- suggests that nuclear migration and neuronal migration are related [52].

Two widely studied systems are oocytes and fungi in terms of nuclear motility. Sustained os-

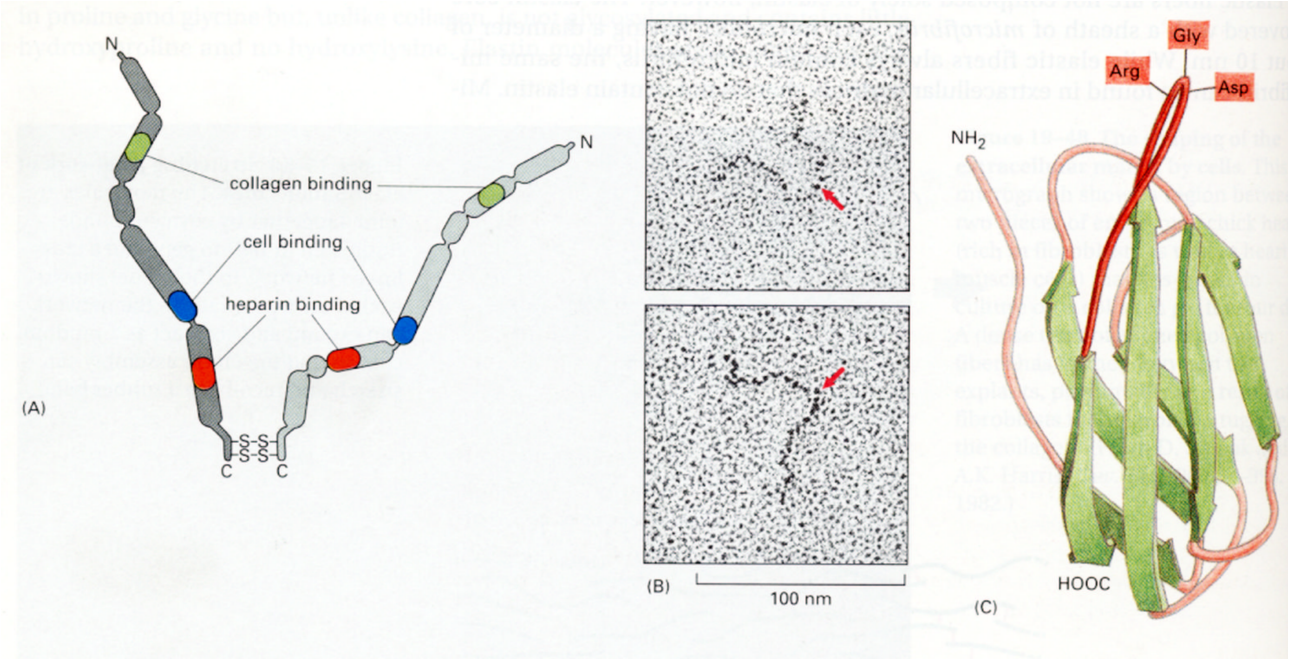

Figure 1.17: The structure of a fibronectin dimer. As shown schematically in (A), the two polypeptide are similar but generally not identical (being made from the same gene but from differently spliced mRNAs). They are joined by two disulfide bonds near the carboxyl terminus. Each chain is almost 2500 amino acid residues long and is folded into five or six rodlike domains connected by flexible polypeptide segments. Individual domains are specialized for binding to a particular molecule or to a cell, as indicated for three of the domains. For simplicity, not all of the known binding sites are shown (there are other cell-binding sites, for example). (B) Electron micrographs of individual molecules shadowed with platinum: *arrows* mark the carboxyl termini. (C) The three-dimensional structure of a type III fibronectin repeat, as determined by nuclear magnetic resonance studies. It is the main type of repeating modules in fibronectin and is also found in many other proteins. The Arg-Gly-Asp (RGD) sequence shown in part of the major cell-binding site (shown in blue in [A]). *(Source: [2], p. 986.)*

cillations of the nucleus between the ends of the cell was found to be driven by MT-polymerization in fission yeast before meiotic division [24]. This phenomenon takes place on the scale of minutes. In this case a bundle of MT-s pushes the microtubule organizing center, which drags the nucleus. Similarly, positioning the nucleus by pushing via MT polymerization in fission yeast has been also described [75]. The rotation of the nucleus was described in several cell types [5]. In culture most of the rotations occur in the plane of the culture dish, i.e. in the plane of the flattened cell. Rotational activity was found to be related to the cell cycle: it happens preferentially in phases that surround mitosis. Interestingly, in the roots of plants nuclei move in an actin- dependent way (e.g. [17]), not by means of MT-polymerization or MT motors.

Experiments in microfabricated chambers showed that the polimerization force of microtubules

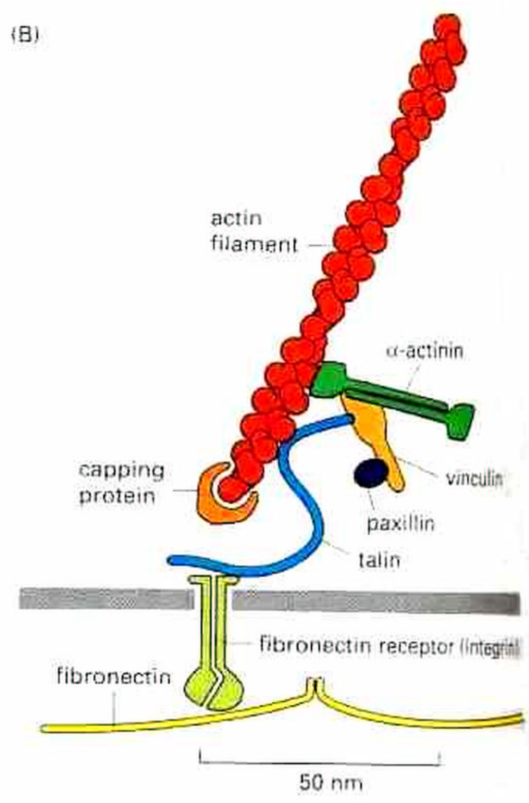

Figure 1.18: A possible arrangement of some of the intracellular attachment proteins that mediate the linkage between an integrin and actin filaments is shown. *(Source: [2], p. 842.)*

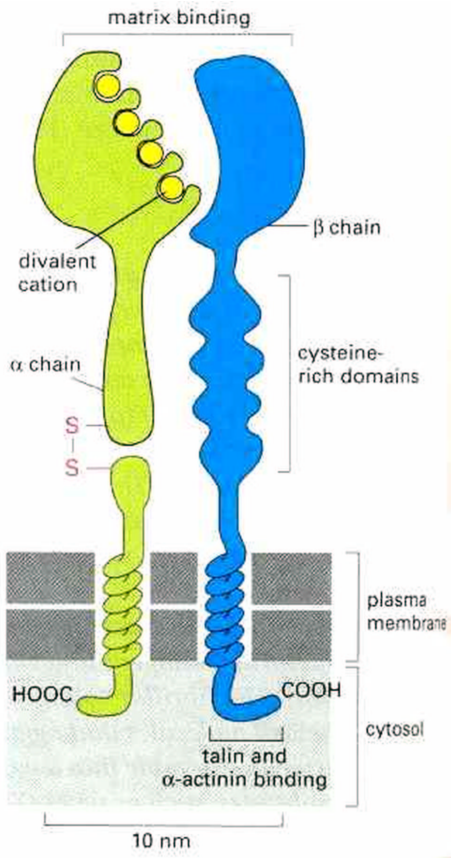

Figure 1.19: The subunit structure of an integrin cell-surface matrix receptor. Electron micrographs of isolated receptors suggest that the molecule has approximately the shape shown, with the globular head projecting more than 20 nm from the lipid bilayer. By binding to a matrix protein outside the cell and to the actin cytoskeleton (via the attachment proteins talin and α-actinin) inside the cell, the protein serves as a transmembrane linker. The α and β chains are both glycosylated (not shown) and are held together by noncovalent bonds. In the fibronectin receptor shown, the α chain is made initially as a single 140,000-dalton polypeptide chain, which is then cleaved into one small transmembrane chain and one large extracellular chain that remain held together by a disulfide bond; this extracellular chain is folded into four divalent-cation-binding domains. The extracellular part of the β chain contains a repeating cysteine-rich region, where interchain disulfide bonding occurs; the β chain has a mass of about 100,000 daltons.

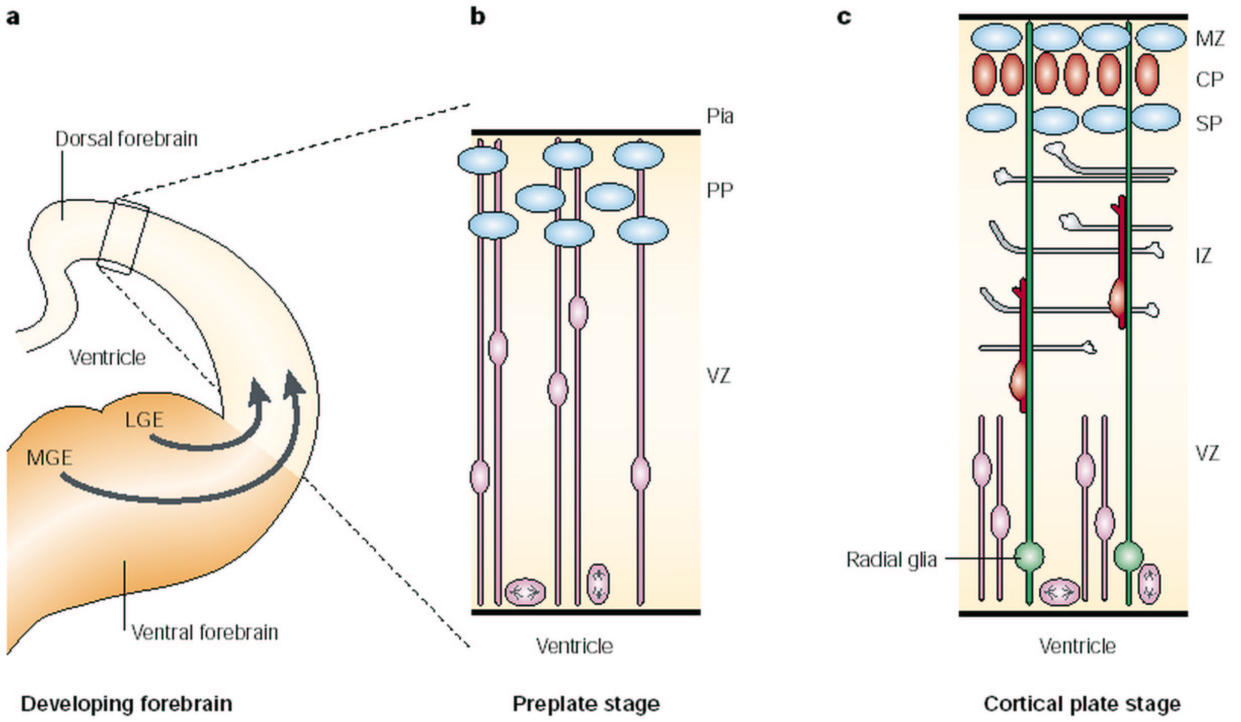

Figure 1.20: **a,** Schematic diagram of a section through the developing rodent forebrain. **b, c,** Illustrations of the different stages of neocortical development. The dorsal forebrain gives rise to the cerebral cortex. The lateral ganglionic eminence (LGE) and medial ganglionic eminence (MGE) of the ventral forebrain generate the neurons of the basal ganglia and the cortical interneurons; the latter follow tangential migratory routes to the cortex (**a,** arrows). In the dorsal forebrain (**a,** boxed area), neuronal migration begins when the first cohort of postmitotic neurons moves out of the ventricular zone (VZ) to form the preplate (PP) **(b)**. Subsequent cohorts of neurons (pyramidal cells) migrate, aided by radial glia, through the intermediate zone (IZ) to split the PP into the outer marginal zone (MZ) and inner subplate (SP) **(c)**. CP, cortical plate. *Source: [56]*

itself in the absence of motors (dynein and kinesin) could position the artificial centrosome in the middle of the MT asters to the geometric center of the chamber [38]. Dynamic instability of MT-s enables the centrosome to explore the chamber geometry [30]. Theoretical results reinforce that the centrosome can be driven by the pushing force of polymerizing MT-s in a simple way [25].

1.5.1 Cell polarization and centrosomes in motile cells

The polarization of cells is a poorly understood phenomenon, and it is being explored by the tools of molecular biology. Polarization is crucial in numerous cell types. In polarized cells the spatial distribution of intracellular molecules is asymmetric. MT-s and centrosomes are known to have central role in polarization. The correlation between the position of centrosomes and polarization is far from trivial. In motile cells the direction of migration and the position of centrosomes seem to be related in a not yet clear way [80] [21] [57].

Chapter 2

Objectives

Motion of cell components is dominated by random positional fluctuations and periodic movement on the scale of biomolecules. Cell motility and shape formation are believed to be directly related to the polymerization dynamics of actin and actin-associated motor proteins. Sophisticated theoretical models and a number of ingenious experiments have provided strong evidence that cell protrusion is driven by actin polymerization, e.g., [51, 1]. Although several experiments have been carried out in order to understand the precise mechanism of cellular motility, the detailed process is still uncovered, especially on the nanometer scale.

Fluctuations are considered to be crucial in terms of the understanding of cellular motility. In principle, nanometer scale fluctuations of cells can be studied by the atomic force microscope (AFM), and this technique is almost unique in this sense. (In some cases, fluctuations of biopolymers, such as F-actin, can be visualized also by special optical microscopes [22] beneath the micron range.) We attempted to probe these fluctuations with the AFM. Our purpose was to gain deeper insight into the dynamics of cells than an optical microscope could ever provide.

Microscopic fluctuations result in controlled macroscopic biological motility. We studied a type of intracellular motion, which is mesoscopic in this sence: motility of the cell nucleus shows both stochastic and controlled features.

Nuclear migration is an essential aspect of a number of cellular and developmental processes. Appropriate location of the nucleus even in non-M phase cells can be relevant. For example, in the tightly packed pseudostratified epithelia nuclei of the elongated cells are arranged to avoid each other [69]. Migrating cultured cells translocate their cell bodies to the leading edge by nucleokinesis [43]. In the developing brain distinct modes of neuronal migration are known [56]; in the ventricular zone nuclei of neuronal progenitor cells and radial glial cells oscillate between the borders of the zone (1.20). Although it has important role in the development of the brain [54], the function and mechanism of this remarkable phenomenon called interkinetic nuclear migration is not clear.

Experimental systems used to investigate nuclear motility mentioned above and in the introduc-

tion could not reveal the biophysical mechanism that drives long-term nuclear migration in animal cells. Using a micropatterning technique combined with time lapse phase contrast microscopy and subsequent protein labeling we were looking for this mechanism. Our aim was to quantitatively describe the phenomenon of nuclear migration in elongated cells and give a reasonable physical model, which can explain the effect in agreement with former results and our experimental observations.

Chapter 3

Materials and Methods

3.1 Cell cultures: in vitro environment

Most animal cells are adherent, which means that they can survive if they are attached to a solid surface. There are a few exceptions e.g., red blood cells. Adherent cells can be maintained in vitro on numerous surfaces such as glass in the appropriate culture medium. Although artificial surfaces that are used to keep cells in vitro can only partially mimic the natural environment of cells, these cultures can be reasonable models of tissues.

Cells can be kept alive for a few hours in physiological buffers that are solutions of salts. On the long run they need culture medium and some components of the blood serum to live and proliferate sufficiently. These components are proteins, especially growth factors, which are present in the physiological environment of cells in tissues. Numerous different culture media are known. They consist of water, salts, amino acids, glucose and vitamins. Which medium to choose depends on the cell type and the experimental setup. We used DMEM (Dulbecco's Modified Eagle Medium) with 10 % FCS (Fetal Calf Serum) in the AFM experiments and MEM (Minimal Essential Medium) with 10 % FCS in the time-lapse phase contrast experiments. Mammalian cells need 37 °C. For a short time they can survive at lower temperatures (e.g. room temperature) without any irreversible damage. For a practically infinite period of time cells can be kept in a frozen state using liquid nitrogen and a cryoprotective agent (e.g. DMSO or glycerol). Transition from 37 °C to -196 °C and backwards can be lethal, in most cases a number of cells will not survive. This is called freeze-thaw damage. Interestingly, a relatively slow freezing process from 37 °C to about -60 ° is more successful than a rapid one. pH of the medium can be stabilized in 5% CO_2 atmosphere. CO_2 diffuses into the medium from the atmosphere.

We used several types of cells in our experiments: 3T3 mouse fibroblast [74], C6 rat glioma [7], U87 human glioma [62] immortalized cell lines and primary mouse fibroblasts.

Cultures of C6, U87, and 3T3 cells were grown in DMEM (Dulbecco's Modified Eagle Medium,

GIBCO) or MEM (Minimum Essential Medium, SIGMA) supplemented with 10 % fetal calf serum (FCS; Gibco), 4 mM glutamine and 40 μg/ml gentamycin in humidified air atmosphere containing 5% CO_2, at 37 °C. Primary fibroblasts were isolated from the bodies of 13 day old mouse embryos. Primary astroglial cells were prepared from newborn mouse forebrains, as it was described previously [44].

3.2 Atomic force microscopy

3.2.1 Fundamentals

Atomic Force Microscopy (AFM) is a relatively new technique that belongs to the family of scanning probe microscopes (SPM-s). SPM-s employ a microscopic probe, which scans over the surface being investigated. Positioning the probe with 0.01 nm accuracy can be solved by using a piezo electric scanner. Differences between SPM-s emerge from the interaction between the surface and the probe. An electrical feedback circuit can be used to keep the strength of the interaction at a constant level, which, in turn, makes it possible to acquire a map of the surface.

The first SPM, invented and constructed in 1981-82 by Binnig and Rohrer [9], was a scanning tunneling microscope (STM). This technique is capable of the examination of electrically conducting surfaces on an atomic scale. Due to the voltage applied to the probe, which is a sharp conducting tip in this case, tunneling current flows from the tip to the sample or vice versa. The tunneling current is usually an exponential function of the distance between the tip and the sample [68] with a characteristic distance in the range of 0.01 nm. This is the main feature of the technique that makes atomic resolution possible. Most biological samples can hardly be probed by STM due to their insulating character. AFM solves this problem effectively [8, 48]. Probe of the AFM is a sharp hard tip, which can be either an electric conductor or an insulator. The tip is mounted on a cantilever (spring). A single carbon nanotube can be either grown or attached to the end of the tip, resulting in an extremely high aspect-ratio and a small radius of curvature (Fig. 3.1).

AFM is a force sensor. When the surface under investigation attracts or repels the tip, the cantilever bends to or from the surface. This bending is then measured by position sensitive photo diodes *via* the displacement of the laser beam reflected by the back of the cantilever. (Fig. 3.2.)

With this technique the cantilever's deflection can be sensed with a 0.01 nm resolution. Force between the sample and the tip is determined according to Hooke's law, if the force constant of the cantilever is known. Thermal vibrations of the cantilever provide an elegant tool to measure its force constant [46]. Although further methods are also available, this technique is the most practical. Some commercial AFM softwares can do the force calibration with high precision automatically using the thermal fluctuation method.

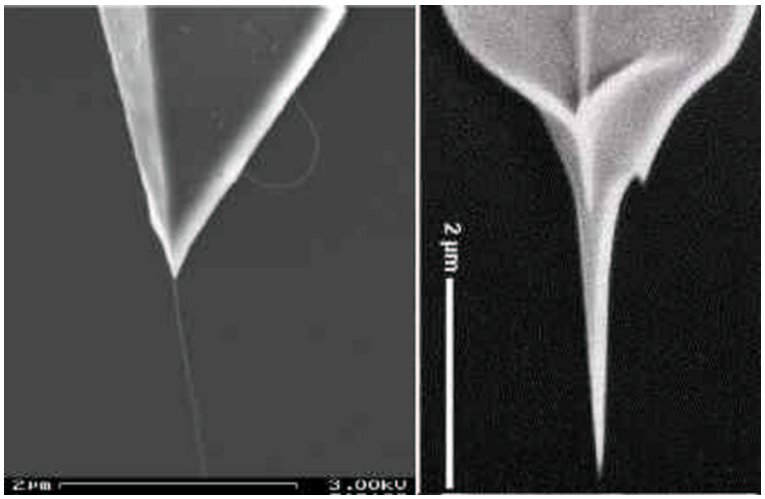

Figure 3.1: Scanning electron micrographs: an etched silicon tip on the right and a carbon nanotube probe on the left. *(Source: http://store.veco.com and http://cmliris.harvard.edu/.)*

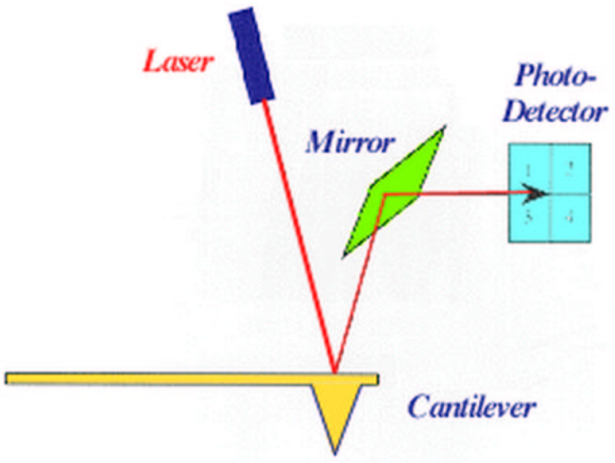

Figure 3.2: Schematic representation of the AFM head. Beam emitted from a laser diode is reflected on the back of the cantilever. With the help of an adjustable mirror the laser beam can be directed to the photo diodes. Bending of the cantilever is measured by the detection of the position of the laser spot on the surface of the diodes. The photodetector is made up of 4 segments: not only the bending but the torsition of the cantilever can be measured, as well.

Piezo scanners actuate the cantilever. When high voltage is applied to a piezoelectric material, it elongates. This effect is utilized in the scanners (Fig. 3.3). Piezo scanners can position the tip attached to them with an accuracy in the 0.01 nm range. Difficulties appear with distortion, reproducibility, and accuracy of measurements due to the nonlinearity, hysteresis, and drift of the piezo effect.

Sensitivity and resolution of AFM is determined by distinct parameters: the intrinsic sensitivity of the optical lever; thermal noise; and the tip's radius of curvature. (See $http://green.la.asu.edu/review/chap_2.htm$ and references therein.) Best resolution that can be achieved on the surface of living cells is in the range of 10-100 nm. Higher resolution images will not reveal more details due to the low contrast, which is an outcome of the softness.

3.2.2 Imaging and spectroscopy

The imaging ability of AFM is utilized in numerous fields of surface science and solid state physics. AFM also has industrial applications e.g., in semiconductor technology. In biology it is applied for both imaging and spectroscopic purposes.

The two basic modes of AFM imaging are contact mode and non-contact (tapping) mode [34]. In contact mode the tip is in continuous contact with the sample, i.e., it is in the repelling zone of the van der Waals interaction. On the contrary, in tapping mode the tip oscillates with high frequency in the attractive zone (farther from the sample surface) and hits the surface once in a period. In contact mode AFM acquires the equiforce map of the surface using an electric feedback loop that adjusts the z coordinate (perpendicular direction to the surface) of the cantilever so that the force would be constant. This 3D map is called contact mode topographic image. Feedback parameters can be tuned. Perfect feedback would result in a constant deflection of the tip. In deflection mode AFM measures the deflection of the cantilever, i.e., the error of the feedback. Deflection mode images usually give better contrast than the topographic ones due to the high deflection of the cantilever at the edges on the surface. Finite time constant of the feedback limits the scanning speed. Generally, the frequency of the scanning is kept constant, when the scanned area changes: scanning speed is higher in a larger window. The optimal scanning frequency is determined mainly by the piezo scanner itself. In tapping mode either the amplitude or the phase of the oscillation is kept constant by feedback. Far from the sample the operator adjusts the excitation frequency (frequency of the AC on the piezo oscillating it in the z direction) close to a resonant peak of the cantilever. In the proximity of the sample both the amplitude and phase of the oscillation is altered by the interaction between the tip and the surface. Constant force gradient map of the surface can be imaged by this method because the eigenfrequency of the cantilever is dependent on the z gradient of the tip-sample force. Investigating soft biological samples, tapping mode is very useful since it is more gentle than the contact mode: deforms or damages the sample in a less extent.

Spatial resolution provided by optical microscopy of living cells does not enable researchers to

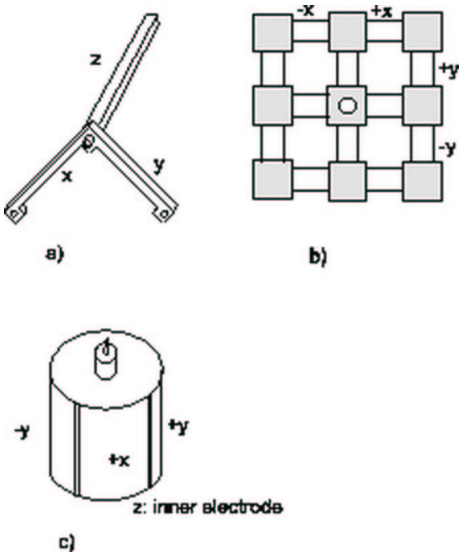

Figure 3.3: Types of piezo scanners: a, the tripod; b, the thermally compensated symmetrical scanner and c, the piezo tube. The first STMs all used piezo tripods for scanning. The piezo tripod is an intuitive way to generate the three dimensional movement of a tip attached to its center. However, to get a suitable stability and scanning range, the tripod needs to be fairly large (about 5 cm). Its size and its asymmetric shape make it very susceptible to thermal drift. The thermal drift performance of the symmetrical design is much better than the simple tripod. However a complicated assembly of many piezo pieces is required. The tube scanner is now widely used in SPM for its simplicity and its small size. The outer electrode is segmented in four equal sectors of 90 degrees. Opposite sectors are driven by signals of the same magnitude, but opposite sign. This gives, through bending, a two dimensional movement on, approximately, a sphere. The inner electrode is normally driven by the z signal. It is possible, however, to use only the outer electrodes for scanning and for the z movement. The main drawback of applying the z signal to the outer electrodes is, that the applied voltage is the sum of both the x or y movement and the z-movement. Hence a larger scan size effectively reduces the available range for the z control. Piezo scanners, tubes and tripods, are made of piezo ceramic material. Piezo materials with a high conversion ratio or small distances between the electrodes, allowing large scan ranges with low driving voltages, do have substantial hysteresis resulting in a deviation from linearity by more than 10%. The sensitivity of the piezo ceramic material (mechanical displacement divided by driving voltage) increases with reduced scanning range, whereas the hysteresis is reduced. A careful selection of the material for the piezo scanners, the design of the scanners, and of the operating conditions is necessary to get optimum performance. *Source:* $http : //wwwex.physik.uni - ulm.de/lehre/PhysikalischeElektronik/Phys_Elektr/node236.html$

observe nanometer scale motion and rearrangement of cell components. AFM is an adequate tool for such measurements [14, 36, 58, 65]. Stress fibres (contractile bundles of actin filaments and myosin-II) play an important role in the control of cell shape and the adhesion of cells to the extracellular matrix through focal contacts. These characteristic cytoskeletal elements can be imaged with the AFM due to their high elastic modulus [64, 37]. AFM is capable not only for recording high-resolution topographic images of living cells but also for measuring the elastic properties of them simultaneously [45] and investigating cellular dynamics [26, 66].

Positioning the tip over a point of the sample, force-distance curves can be acquired by approaching and removing the tip from the surface. These curves -also named force spectra- can be highly informative in terms of the local elastic properties of the sample. Elastic modulus of the sample can be calculated from the force spectra in case of a living cell, too (e.g. [45, 33]. Local force spectroscopy on each pixel of an image will provide the elastic map of the surface.

The main field of application of force spectroscopy is the study of intra- or intermolecular interactions with pN and subnanometer resolution (for review see [81]). Among others, protein folding, receptor binding, antibody-antigen and DNA-protein interactions can be studied by this technique.

3.2.3 Technical details

Scanning repetitively the surface of a cell time-lapse images can be recorded [33, 67]. The analysis of subsequent images yielding a movie is highly informative in terms of the kinetics of the cytoskeleton. Although fast cellular motility can not be examined by the repetitive scanning procedure due to the minute-range of scanning time, nanometer scale fast motion can be probed by positioning the tip on the area of interest. In this way we could investigate the fast vertical fluctuations of the cells.

A commercial AFM (TopoMetrix Explorer, Santa Clara, CA) with a tripod piezo scanner and custom-made sample heating control system and fluid chamber was used (Fig. 3.4 and 3.5). Measurements were carried out at 37 °C in CO_2 independent medium containing 10% fetal calf serum (GIBCO). We used soft silicon nitride cantilevers (Thermomicroscopes, Coated Sharp Microlevers, Model # MSCT-AUHW, with typical force constant 0.01–0.03 N/m, 20 nm radius of curvature). Topographic and deflection images were acquired in contact mode. High-resolution images were acquired at a scanning frequency of $\sim$4 Hz. Non-destructive low force scanning provided stable sustained imaging of living cells for 8–10 hours. After the AFM experiments cells were maintained in the same medium for 1–2 days and found to be normal. We could not achieve high-resolution imaging on a portion of cells due to their increased height or softness.

Considering that small details of cellular components can be observed at the best quality on shaded deflection mode images we present our experimental data in this format. Topographic images provide height information but with poor contrast.

We measured the average displacement of the contour at the edges of cells. In the middle of cells

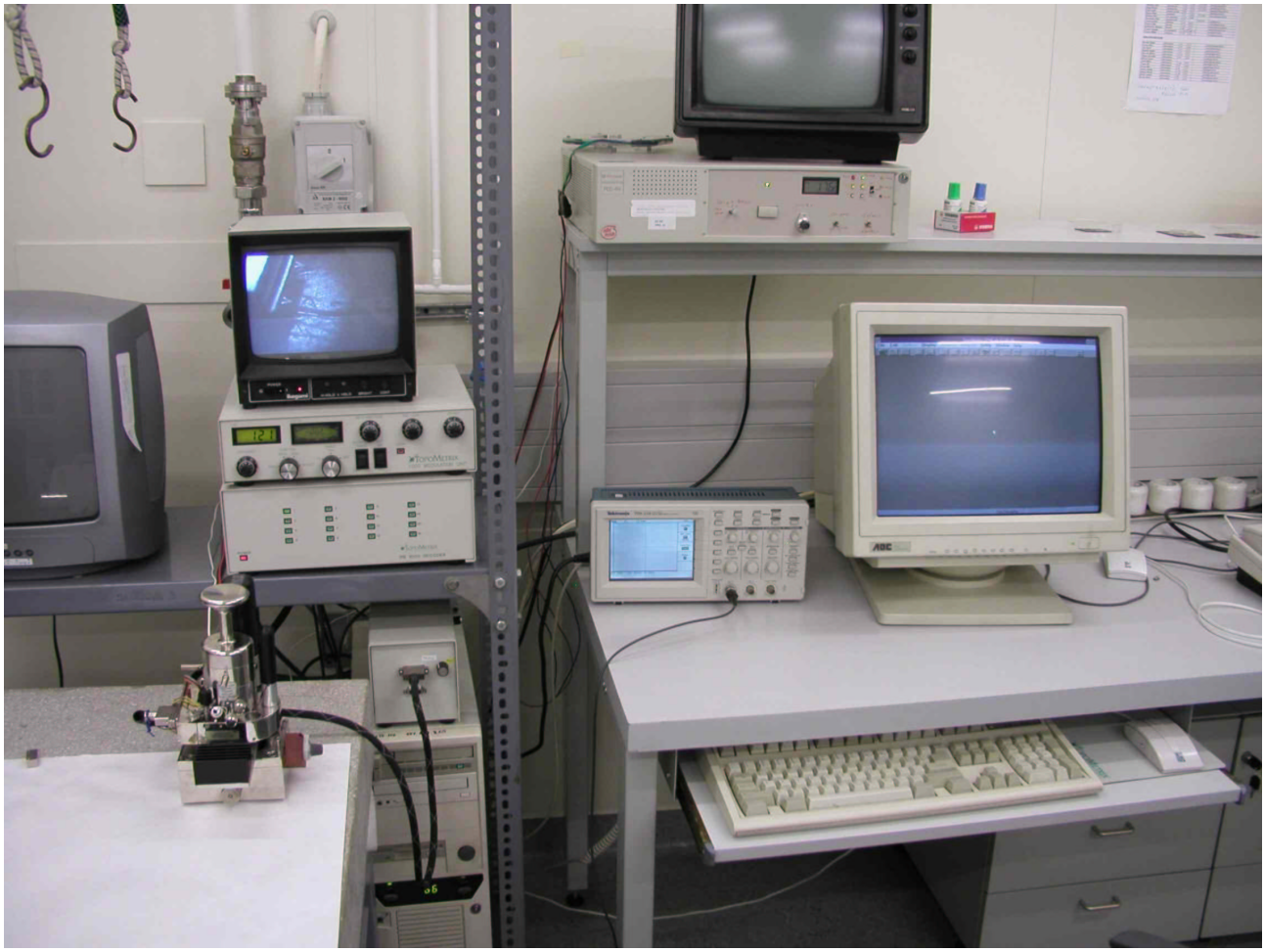

Figure 3.4: The AFM system we used. AFM head on the vibration isolated stage on the lower left, above this the monitor -showing the position of the tips and the sample- on the top of the AFM control boxes, the heating control on the top middle, under this the digital oscilloscope, and the pc monitor beside.

Figure 3.5: TopoMetrix AFM head on the home-made heat controlled sample holder.

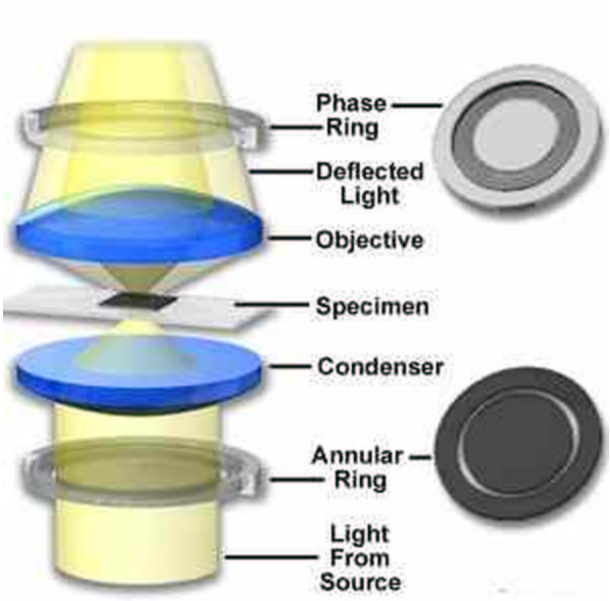

Figure 3.6: Phase contrast light pathways in an upright arrangement. *(Source: http://www.olympusmicro.com/primer/techniques/phasecontrast/phase.html)*

we have chosen some structures with a characteristic shape and the lateral displacements of these structures were measured. The measurement of local height fluctuations of cells was started at least 1/2 h after mounting the sample into the fluid cell. In this way thermal transient effects could be eliminated. After each scan the tip was positioned onto the point of interest with the same force and feedback parameters and we captured the dc voltage of the z piezo by a digital oscilloscope (Tektronix TDS 210) for 22.5 sec with 100 Hz sampling rate.

3.3 Phase contrast time-lapse microscopy

Although most animal cells cannot be visualized by a simple optical microscope since they are transparent, they can be studied by phase contrast microscopy constructed by Zernike in 1932. Phase contrast microscope gives contrast between areas with different refraction indices. The refraction index of the cytoplasm is higher than that of the culture medium. Even some cellular organelles, such as the nucleus can be distinguished by this technique. The main feature of a phase contrast microscope is the special objective with a phase ring and the corresponding illumination through an annular ring (Fig. 3.6). To achieve optimal contrast in case of sample regions with slightly different refraction indices the phase ring is manufactured to cause a $\pi/4$ phase shift of the direct beam. The interference of the direct beam and beams diffracted by the cells results in bright image of the cells with dark background.

On the basis of former videomicroscopes constructed by András Czirók and Balázs Hegedűs,

Figure 3.7: The automated time-lapse inverse phase contrast microscope system we used in the cell motility studies capable for taking high resolution photos of living cells for several days.

which proved to be adequate for the study of cellular locomotion [20, 35] we built an automatic system to acquire time-lapse images (Fig. 3.7). An Olympus C-4040 Zoom digital camera controlled by a computer has been mounted on the side port of a Leica DM IRB inverted microscope with the use of an optical coupling constructed by Ottó Haimann. The communication module of the camera was made by Dávid Selmeczi, it combines the photopc and gphoto2 programs. The focus of the microscope can be automatically adjusted by a computer controlled stepper motor manufactured by Sándor Hopp.

A home-made thermostat constructed by András Czirók and Tamás Vicsek was used to keep the cell cultures at 37 °C. 5% CO_2, 76% nitrogen, 19% oxygen atmosphere and 100% relative humidity was maintained by the application of a computer controlled electrical valve, which controls the in-flow of the fresh 5% CO2 into the thermostat, and open water tanks inside. Prior to the time-lapse experiments cells were passaged over the micropatterned surface of 35 mm plastic petri dishes (Greiner) at a density of 1-1.5 x 10^4 cell/cm^2 in MEM with 10% FCS.

Drugs used in the inhibitor studies: vinblastine, taxol, sodium-orthovanadate, AMP-PNP, cytochalasin D, ML-7 were purchased from SIGMA. Drugs were added to the culture medium after 1-d time-lapse observation of the cells.

3.4 Processing and analysis of data from time-lapse microscopy

Position of the nuclei, and the two ends of single cells showing clear nuclear migration was determined manually in every time-lapse frame using the *gtrak* software constructed by Dávid Selmeczi, wherefrom $x_n(i,t), x_l(i,t)$ and $x_r(i,t)$, location of the nucleus (n) and the two ends (l, r) of the ith cell at time t was defined. Velocity $v_n(i,t)$ of the nucleus of the ith cell at time t was calculated as the net displacement of the nucleus in a time interval of 30 minutes. The start and the end of this interval was chosen symmetrically, 15 minutes before and after the time moment t. Direction of nuclear motility was determined automatically by least squares method. Density function of the velocity $v(n)$ distribution in a cell population was determined as the number n of each occurent velocities v, normalized by the number of velocity data (Σn). Period of the periodic nuclear migration of a certain cell i, was calculated from the $x_n(i,t)$ function by measuring the distance between the peaks. Accuracy of this procedure was $\sim$0.5 h. (Fourier spectrum provided less accurate data of the period if it was close to the time period of observation.)

3.5 Immunocytochemistry

At the end of the time-lapse experiments samples were fixed using 4% paraformaldehyde in PBS for 25 minutes, afterwards kept at 4 °C in PBS containing Na-azide. The membranes of fixed cells were permeabilized by treatment with Triton X-100 (5 min., 0,1% v/v in PBS). Non-specific antibody binding was blocked by incubation with 5 % FCS in PBS at room temperature, for 1 hour. Antibodies to α-tubulin (mouse; ExBio, Praha) and γ-tubulin (rabbit; Sigma) were used at dilutions of 1 to 1000-5000, respectively. Secondary antibodies to α-tubulin were Cy3 (1:3000, Jackson) or Alexa488 labeled anti-mouse IgG-s (1:1000, Molecular Probes). γ-tubulin was visualised by 1.5 hour incubation with biotin-conjugated anti-rabbit IgG (1:1000, Vector) followed by 1 hour incubation with fluorescent avidin-TRITC (1:750, Sigma).

Fluorescent images were aquired with the Leica DM IRB microscope, 40x N-plan objective, mercury lamp illumination or with an Olympus BX61 confocal microscope, 60x oil immersion objective, 1.1 numeric aperture.

3.6 Micropatterned cell adhesive surfaces

We manufactured micropatterned substrates [50] for the phase contrast cell motility studies. Poly-dimethyl-siloxane (DPMS, Sylgard 184 from Dow Corning) micropatterned stamps were fabricated by Gábor Csúcs, Laboratory for Biomechanics, Department for Mechanical and Process Engineering, ETH Zürich with a lithographic procedure [19]. In our nuclear migration studies we used simple striped patterns with 20, 40 or 60 μm lattice constant (Fig. 3.8).

We applied a protein masking technique using poly-l-lysine-poly-ethylene-glycol (PLL-PEG), a molecule repelling proteins. After patterning the substrate surface with the protein we dropped PLL-PEG solution onto it. PLL-PEG adheres to those sites only, where the protein mask does not cover the surface. Cells adhere to the surface via proteins, which infers that they will not adhere to the PLL-PEG covered region but to the protein covered sites.

Either protein solution (40 μg/ml fibronectin, 20 μg/ml Alexa488 (Molecular Probes) labeled fibrinogen) or 50 μg/ml FITC labeled poly-l-lysine (SIGMA) in PBS were placed onto the clean surface of the DPMS stamps for 30 min. Drop was removed and the surface was dried in air flow. We placed the stamp carefully with its patterned face downside on the inner side of the bottom of a 35 mm plastic petri dish or a glass cover slip and pushed it gently to achieve full contact between the stamp and the surface. After 10-20 sec we removed the stamp, and washed the surface with water and HEPES buffer. The quality of the pattern was controlled in the fluorescent microscope (Fig. 3.8). We incubated the surface with 1 mg/ml PLL-PEG in HEPES buffer for 10 min, removed it, and washed the surface with PBS. 1-1.5 10^5 cells in 2.5 ml minimal essential medium (MEM), 10% fetal calf serum (FCS) were passed over the patterned substrate.

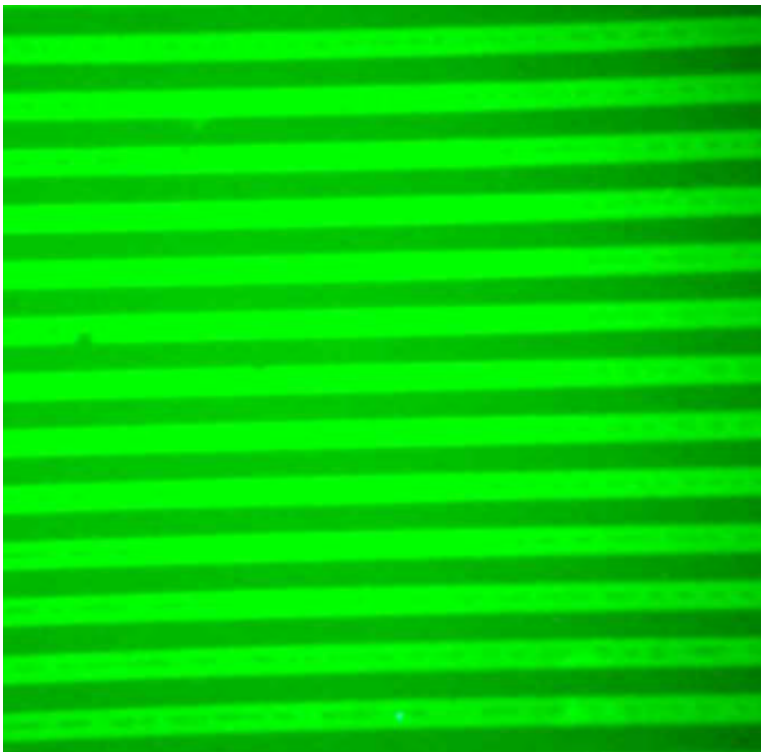

Figure 3.8: Fluorescent protein (fibronectin-Alexa488 labeled fibrinogen mixture) pattern on the surface of a plastic petri dish: 20 μm wide stripes.

Chapter 4

Results

4.1 Nanometer scale cellular fluctuations studied by AFM

We investigated the nanometer scale height fluctuations of 3T3 fibroblast cells by atomic force microscope (AFM) under physiological conditions. Distinct types of cellular motility could be examined by the measurement of vertical fluctuations.

Fig. 4.1 displays 2 images of a movie showing the slight motility of the rear edge of a cell with a 4.5 minutes time shift. This cell was almost quiescent during the experiment with a highly stable structure of cytoskeletal fibers and moderate lateral motility. The rear edge is being pulled by the stress fibres: see the parallel set of curved fibres anchored to the edge of the cell. In the same time cell-matrix junctions or nonspecific contacts adhering the rear of the cell to the support weaken and break. We also observed a typical retracting triangular shaped 20 μm wide contact (image not shown) of the same cell at the rear edge. The contact was broken a few minutes after recording the vertical fluctuations.

Typical vertical fluctuations registered on these two locations are presented in Fig. 4.2. We suppose that the apparent difference between vertical fluctuations originates in the different biological activities of the two regions. While the entire region of the cell shown in Fig. 4.1 was extremely stable with a lateral velocity of about 2 nm/s, the edge beside the retracting triangular shaped contact moved with a speed of about 11 nm/s.

To analyze height fluctuations we calculated the power spectrum and the height-height correlation function with a maximal τ=5 s time shift of each $x(t)$ height-time curve:

$$y^2(\tau) = \sum_t \frac{\left(x(t) - x(t+\tau)\right)^2}{N},\ t = i\Delta t,\ i = 1..N, \tag{4.1}$$

$$N\Delta t = 22.5 - 5s \tag{4.2}$$

where Δt (10 ms) is the sampling time.

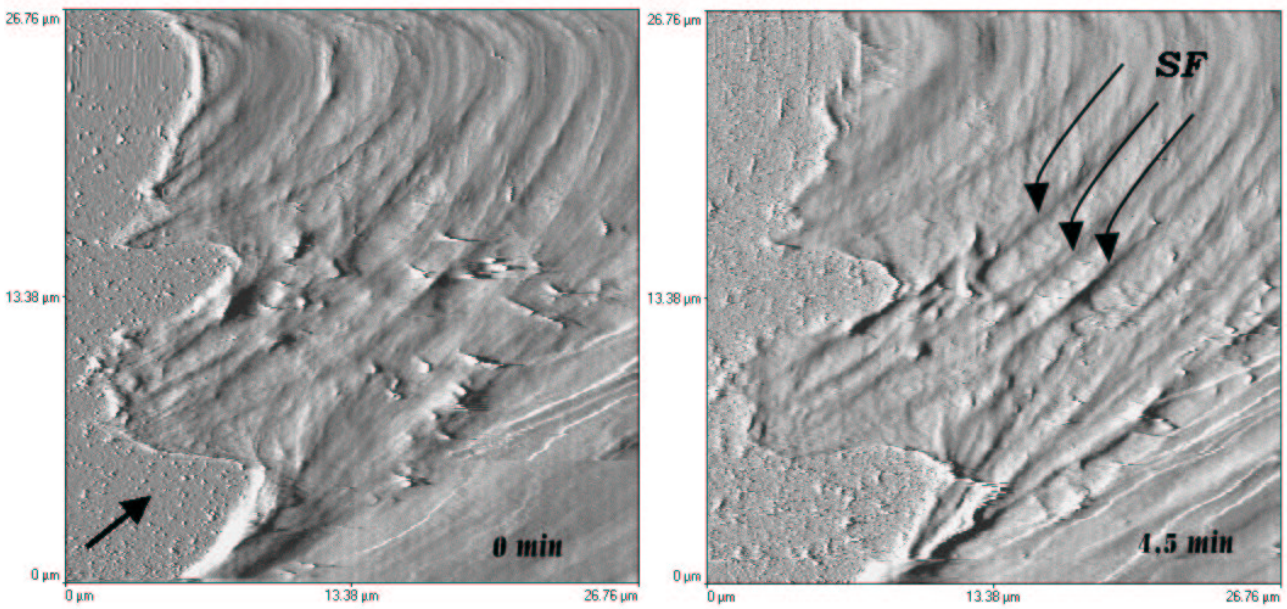

Figure 4.1: Shaded deflection mode images with a 4.5 minutes difference showing stable actin-myosin cables at the rear of a quiescent cell. Arrow in the lower left corner indicates the direction of motion. SF: stress fibres.

This function can characterize stochastic height fluctuations by giving the average change of height as a function of time. Curves are presented in Fig. 4.3, the number of measured height-time curves n is indicated. The lateral velocity of each location seems to correlate with the saturation value of the height-height correlation function measured at that location confirming our assumption that height fluctuations are related to local biological activity (motility). The starting slopes of the curves give the speed of fast fluctuations. Curves saturate with different characteristic (saturation) times. There is an apparent difference between curves (a) and (b) in the saturation value. The characteristic time ($\sim$2 s) of curve (a') is approximately double those of the other two curves. Curve (a') was registered on the middle region (cell body) of the quiescent cell. (See Table 4.1.) Characteristic time and saturation value are related to the average duration and amplitude respectively of an upward or downward motion.

The analysis of power spectra (Fig. 4.4) of the height-time curves acquired on each location of this quiescent cell revealed sustained periodic fluctuations during the experiment (1.5 hours). We found a characteristic peak at 4.9 Hz with a width of 3.5 Hz. The area of this peak gives an average amplitude of 1.5 $\pm$ 0.4 nm. Cells without apparent stress fibres nearby lack this peak. The origin of the sharp peaks in the spectrum is electric noise.

Fig. 4.5 shows the contours of a leading edge of a motile cell from consecutive images. Note the bright spot (S) appearing on the cell surface close to the edge in the middle of the second image. It appears in less than 7 minutes and disappears soon after. A similar one can be observed on the upper

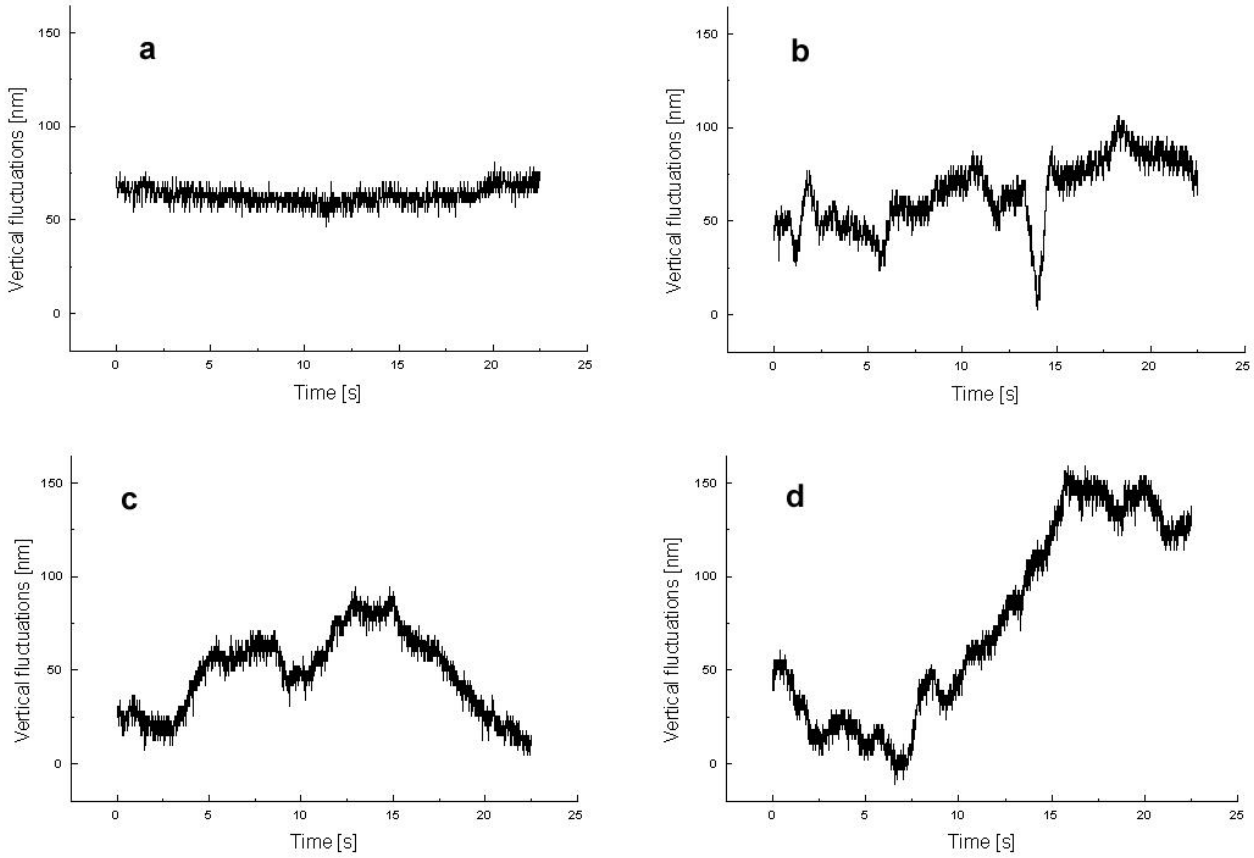

Figure 4.2: Typical vertical fluctuations measured on quiescent and motile cells. Graph (a) and (b) belong to the quiescent, (c) and (d) to the motile cell. We recorded (a) on the rear edge displayed in Fig. 4.1. (b) was measured on a typical retracting triangular shaped contact (image not shown) of the cell at the rear edge. This contact to the support was broken a few minutes after recording the vertical fluctuations. (c) and (d) were registered on the leading edge shown in Fig. 4.5 and close to that on the cell body respectively.

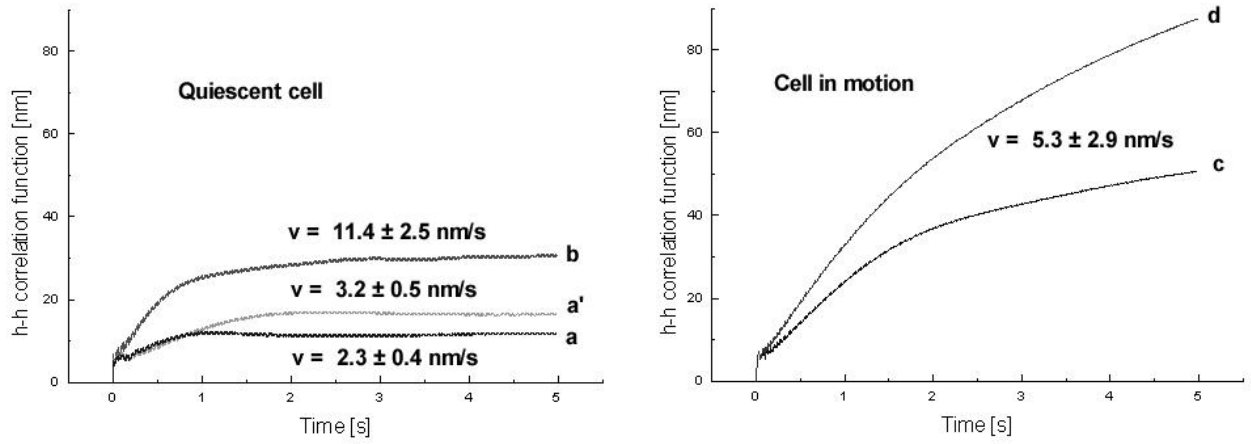

Figure 4.3: Averaged height-height correlation functions of fluctuations measured on the surface of the quiescent and the motile cell. Curves (a, n=10); (b, n=8); (c, n=10) and (d, n=9) are the corresponding correlation functions of vertical fluctuations shown in Fig. 4.2. Curve (a', n=10) was registered on the middle region of the quiescent cell. There is an apparent difference between the behavior of curves belonging to the quiescent and the motile cell. Saturation disappears on the scale of several seconds in case of the motile cell. This fact indicates the presence of vertical motility on this time scale. Significant difference between graph (a) and (b) is attributed to the dynamics of the retracting contact at the rear edge. See the value of lateral velocity of locations at each curve. 50 Hz noise on curves can be observed.

Curve		Starting Slope [nm/s]	r	Saturation value ± SD [nm]	n	Lateral Velocity ± SD [nm/s]
Quiescent cell	a	6.3	0.94	10.5 ± 0.2	10	2.3 ± 0.4
	a'	8.4	0.97	17.0 ± 0.2	10	3.2 ± 0.5
	b	16.7	0.97	28.1 ± 0.3	8	11.4 ± 2.5
Cell in motion	a	20.3	0.998	–	10	5.3 ± 2.9
	b	28.7	0.999	–	9	5.3 ± 2.9

Table 4.1: Comparison of the lateral velocity and parameters characterizing vertical fluctuations of different locations on the quiescent and the motile cell. Parameters of the height-height correlation function are calculated on the basis of curves presented in Fig. 4.3. Starting slope and saturation value were determined by linear fitting in the (0.3 s, 1 s) and (3 s, 5 s) intervals respectively, r: correlation coefficient of fitting, SD: Standard Deviation, n: number of measured height-time curves.

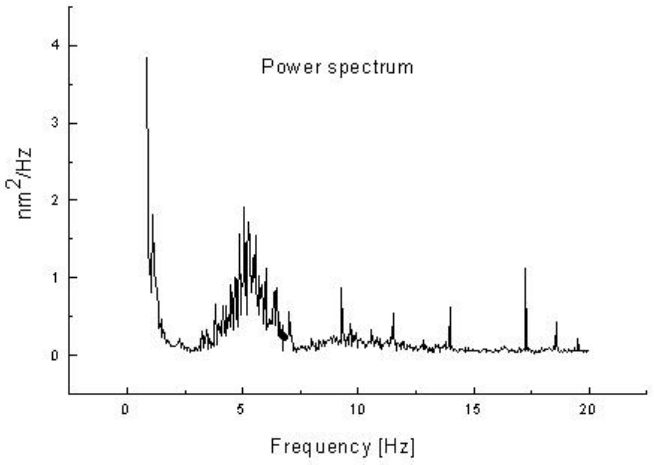

Figure 4.4: Power spectrum (n=10) of height fluctuations measured at the location shown in Fig. 4.1. The peak at 4.9 Hz can be found in each power spectrum of height fluctuations captured on the surface of the quiescent cell. The power spectra of height fluctuations of cells without apparent stress fibres nearby lack this peak.

part of the last image. These features seem to be linked to the ends of curved filaments. In many cases micrometer sized unidentified nodes were found on stress fibres. They might be large protein complexes attached to F-actin.

Fig. 4.2 displays the height-time curves captured on the leading edge (c) and close to that on the cell body (d). Curves show increased motility especially on the long (several seconds) time scale. As a consequence, the saturation effect of the height-height correlation function disappears on this scale (Fig. 4.3). The speed of fast fluctuations is higher, as well. (See Table 4.1.) We suppose that the observed increase in vertical fluctuations is an outcome of actin polymerization-depolymerization processes at the leading edge. Surprisingly, the height-height correlation function shows a higher level of fluctuations farther from the leading edge. It can be a result of actin depolymerization processes well behind the edge or an increased temporal motility of this region which has to follow the edge.

To sum up the results of the fluctuation measurements, correlation could be observed between the heigth fluctuations and the lateral motility of the cells . Fluctuations measured on leading edges appear to be predominantly related to actin polymerization-depolymerization processes. We found fast (5 Hz) pulsatory behavior with 1–2 nm amplitude on a cell with low motility showing emphasized structure of stress fibres. Myosin driven contractions of stress fibres are thought to induce this pulsation [72]

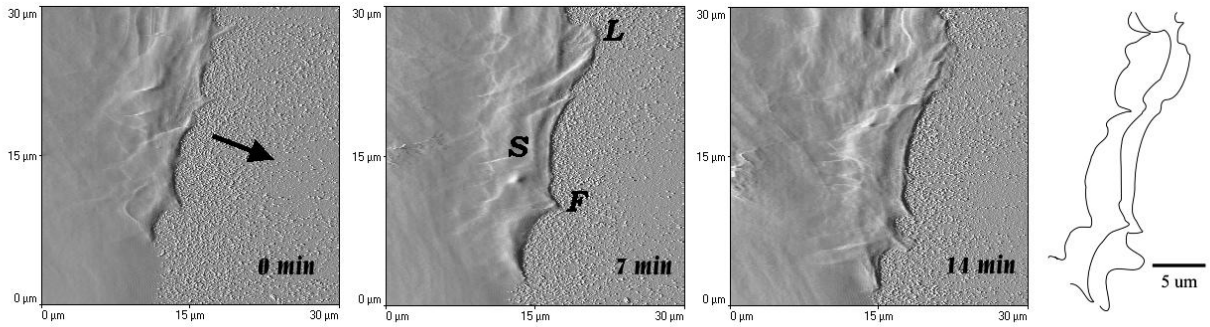

Figure 4.5: Consecutive shaded deflection mode images of a leading edge. Approximately 7 minutes elapsed between images. Arrow indicates the direction of motion. Note the bright spot (S) appearing on the cell surface close to the edge in the middle of the second image. L: lamellipodium, F: filopodium. Contour lines (extreme right) display the forward motion of the edge. The standard deviation of lateral velocity was found to be higher than in the case of a less mobile edge due to extensions growing with high speed, such as the extension on the lower region of the last contour line corresponding to the right hand image.

4.2 Nuclear motility in elongated cells

We used a micropatterning technique to force cells to form highly elongated 'bipolar' shape on narrow adhesive stripes between non-adhesive stripes. This method proved to be adequate to investigate nuclear motility by time-lapse microscopy for several days.

In our nuclear motility experiments, besides U87 human glioma, 3T3 mouse fibroblast and primary mouse fibroblast, we used the C6 rat glioma cell line. This cell line is closely related to the so called radial glial cells that show the phenomenon of interkinetic nuclear migration in the developing brain. Radial-like glial cells could be generated from C6 cells [31]. It means that our experimental setup can be a simple *in vitro* model of cells in the brain in the state of interkinetic nuclear migration. (Interkinetic nuclear migration is coupled to the cell cycle: cells divide after each completed cycle of migration, when the nucleus reaches the end of the cell at the ventricle. This feature is not present in our system.)

4.2.1 Phase contrast movies with subsequent labeling of microtubules and centrosomes

We observed in several experiments that the nucleus of elongated cells on the surface of narrow stripes is motile. This property is general for the investigated cells. Without cell adhesive stripes, cells are not forced to form an elongated shape; they can appear in diverse configurations. Long term migration of the nucleus was observed only in elongated cells, it never happened in cells with variant shapes [71].

We found that the migrating nucleus can turn back at the end of the cell with almost no waiting, and continues to migrate in the opposite direction. Nuclei are able to make numerous cycles in this way (Fig. 4.6). (See demonstrative movies on $http://esr.elte.hu/{\sim}bszabo/dissertation/supplement$ web site.) We call this phenomenon auto-reverse nuclear migration, which is frequent in C6 glioma cells and primary mouse fibroblasts. In fibroblasts the nucleus turns back usually before reaching the end of the elongated cell. Although the nucleus of 3T3 mouse fibroblasts was also motile, it turned back rarely at the end of the elongated cells. Nucleus of U87 human glioma cells was much less motile, which is attributed to their less elongated shape even on the narrow cell adhesive stripes. Average period of periodic nuclear motility in C6 cells (4.6 ± 1.9 hours, 27 analyzed cells) was lower than the period of their cell cycle, which is about 1 day. In case of primary mouse fibroblasts the average period was more than 2 times shorter: 1.8 ± 0.6 hours (6 analyzed cells).

In each time-lapse frame the exact position of the nuclei was identified manually. Only single cells showing clear nuclear migration were analyzed. We determined some statistical parameters that can characterize periodic nuclear migration. Average velocity of migrating nuclei was 29 ± 13 μm/h based on 5 distinct experiments using C6 cells. The total number of analyzed cells was 32. Average velocity of the nuclei showing periodic motion in primary mouse fibroblasts was 26 ± 10 μm/h analyzing 15 cells.

For further studies we used the C6 cell line. Material of the cell adhesive stripes had no significant impact on the motility: fibronectin-fibrinogen and poly-l-lysine stripes gave similar results. Distribution density function of the velocity shows a peak at 0 and a long tail towards the maximal velocity measured in our experiments (Fig. 4.8). As a consequence, standard deviation of the velocity is high, 80% of the average velocity. The ratio of the maximal velocity and average velocity is 6.

At the end of time-lapse experiments we fixed the samples and labeled the centrosomes. Position of centrosomes being the MT organizing centers was considered to be informative in terms of the polarization of the cell since cell polarization is known to be strongly dependent on the MT system. The fact that in polarized, migrating cells the position of the centrosome is cell type specific, i.e., in some cells the centrosome moves in front of the nucleus, in other cells it lags behind it [80], infers that cell polarization is not simply correlated with the position of the centrosome. We found that in C6 rat glioma cells the centrosome stays behind the migrating nucleus, or beside it between the plasma membrane and the nuclear membrane (Fig. 4.9). Labeling of MT-s showed no apparent asymmetry between the leading edge and the tail of cells (Fig. 4.10). MT-s are mainly parallel to the axis of the cell. Fluorescent imaging of MT-s in the highly elongated cells was extremely difficult due to their close packing. (Fig. 4.11.)

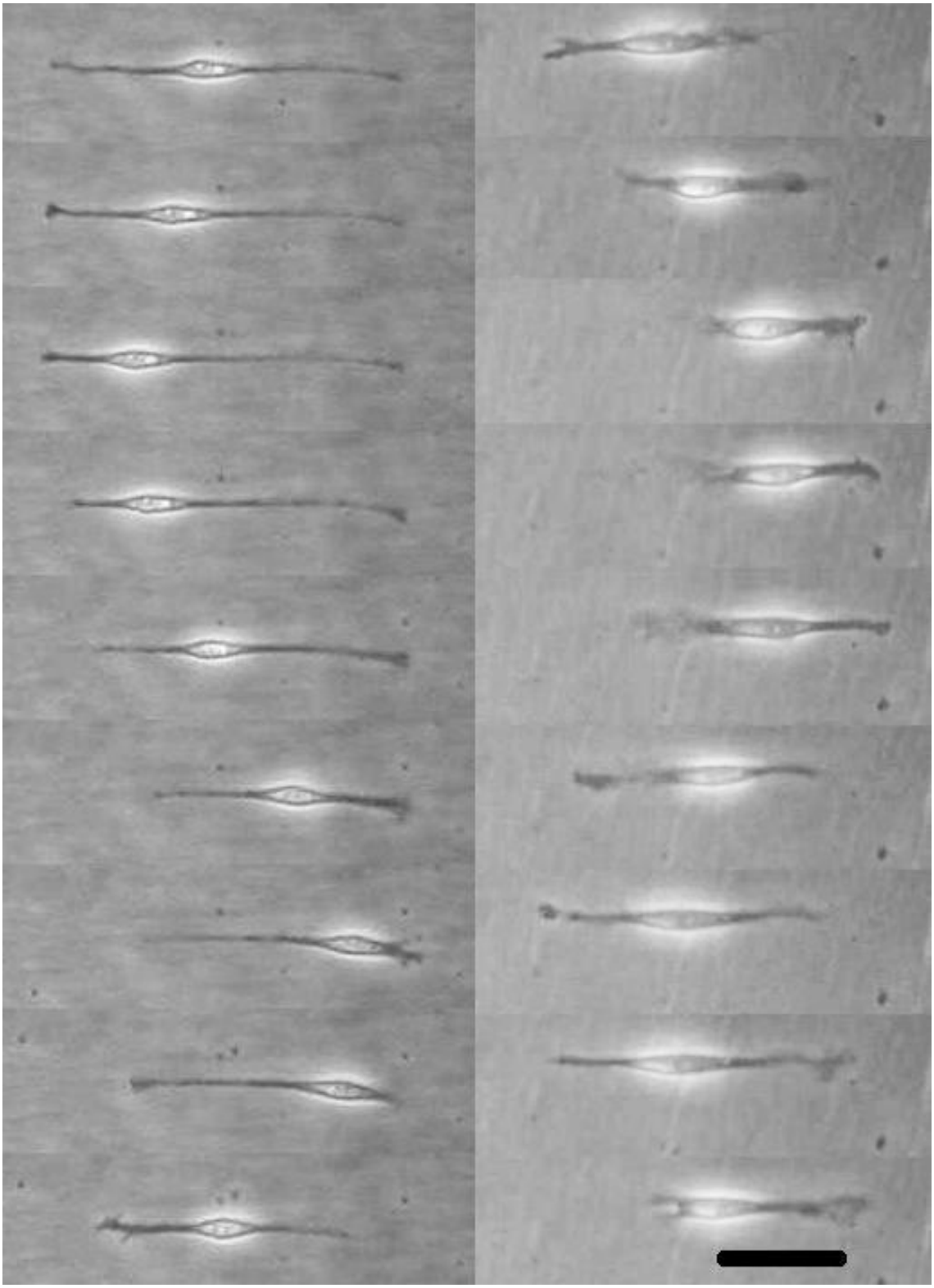

Figure 4.6: Position of the nucleus in a C6 rat glioma cell (left) and in a primary mouse fibroblast (right) during nuclear migration. Time shift is 1 h between subsequent images in case of the C6 cell and 10 min in case of the mouse fibroblast. Note that the frequency of periodic nuclear migration is much higher in case of the fibroblast. Scale bar: 50 μm.

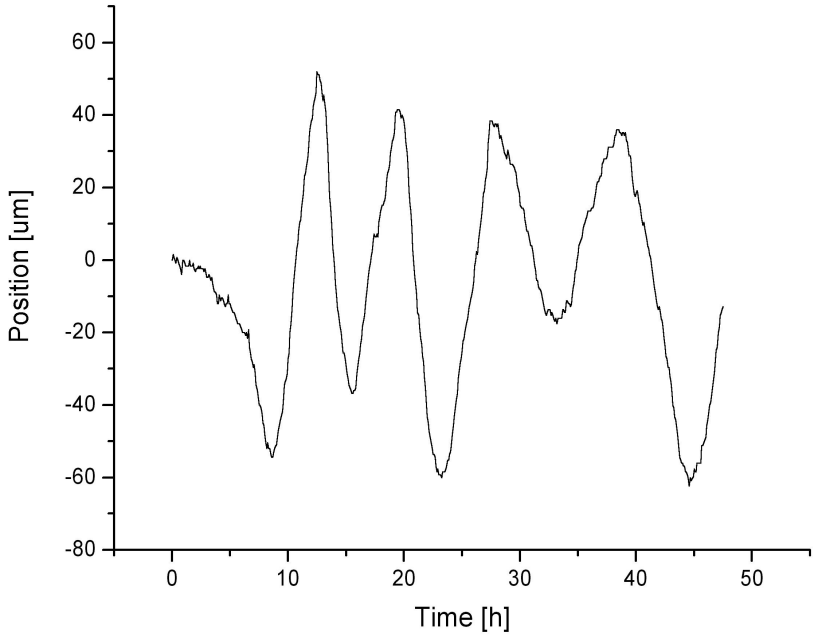

Figure 4.7: Position of the nucleus as a function of time in case of the C6 cell shown in Fig. 4.6.

4.2.2 Inhibitor studies

We targeted the two main force generating cytoskeletal elements: actin- and microtubule-related systems with specific drugs to reveal their roles in nuclear motility.

MT-s were affected by vinblastine and taxol in a concentration-dependent way. Whereas taxol stabilizes MT-s, vinblastine [11, 32] depolymerizes them. Both drugs inhibited nuclear migration even at low concentrations. Taxol was effective above 10 nM, vinblastine blocked the migration of the nucleus at 20 nM. While, in case of vinblastine cells became less elongated, taxol increased the level of elongation, which is in consistence with their opposite impact on MT-s.

MT motors: kinesins and cytoplasmic dyneins were inhibited by 5 μM vanadate and 100 μM AMP-PNP, respectively [39, 55]. Vanadate is an inorganic dynein inhibitor, AMP-PNP is an ATP analogue bound but not hydrolyzed by kinesins. They had no effect on nuclear motility.

Actin was affected by the F-actin disrupting cytochalasin D [73], which had slight effect on the migration of the nuclei at a concentration of 200 nM. Not even 500 nM cytochalasin D blocked nuclear migration, it only decreased the velocity of nuclei. Myosin-II was inhibited by 1 and 10 μM ML-7 [4], a specific MLCK-inhibitor. Surprisingly, ML-7 rather increased nuclear motility at high concentration (Table 4.2).

Cells with migrating nucleus were polarized: a narrow lamellipodium at the leading edge and a tail behind the nucleus could be observed (Fig. 4.6). Polarization of the cell flips as the nucleus

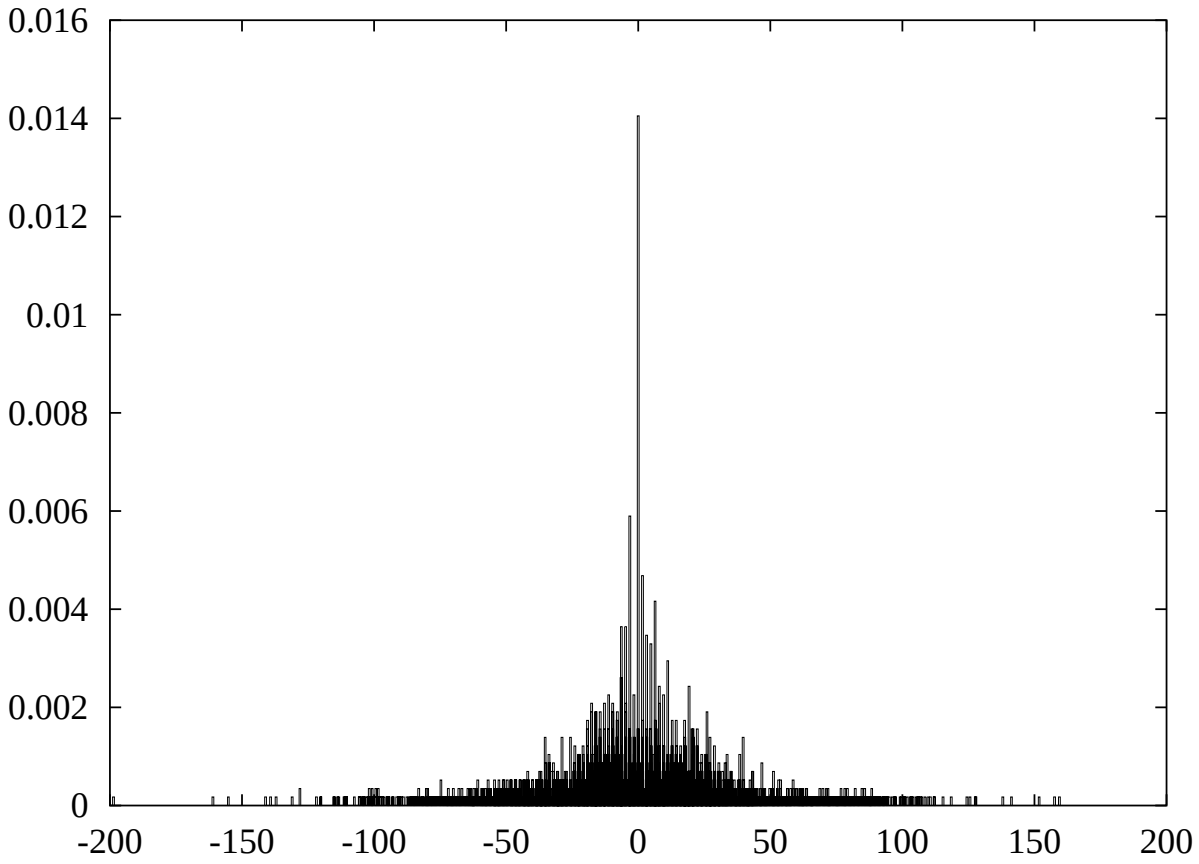

Figure 4.8: Histogram of the density function of velocity distribution of the nucleus in elongated C6 cells showing 'auto-reverse' nuclear migration. This curve is an averaged function of 32 cells from 5 distinct experiments. x scale: μm/h. It shows that the lower velocities are more frequent during nuclear migration, which means that the nucleus does not migrate with a constant velocity. During the reverse at the end of the cell, it moves slowly, and reaches its maximal speed only for a short time at the middle region of the cell.

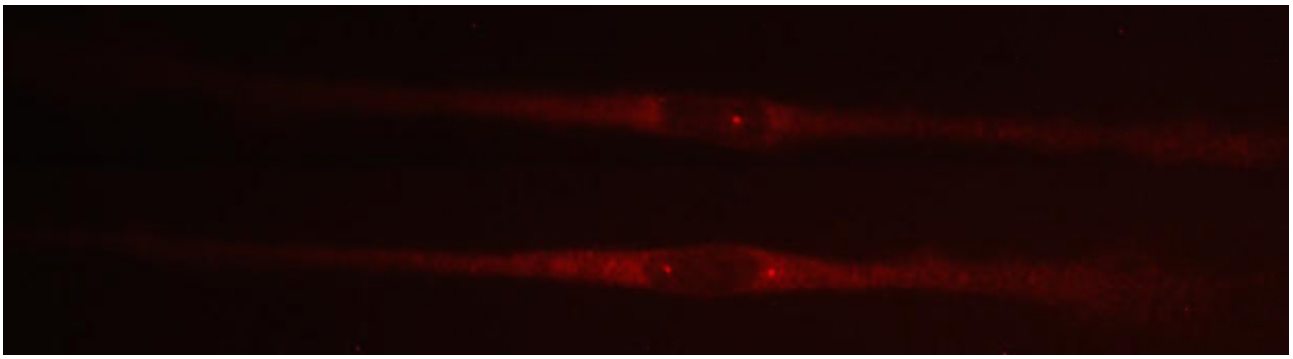

Figure 4.9: Fluorescent images of centrosomes labeled by anti-γ-tubulin in C6 cells after time-lapse microscopy. Nucleus of the upper cell migrated to the left, i.e., its single centrosome stayed at the rear part of the nucleus, which was general in C6 cells. Nucleus of the lower cell did not show migration. Its double centrosomes were arranged towards the ends of the elongated cell. This symmetric arrangement may inhibit nuclear migration. We found motile nuclei with double centrosomes, too. In this case both nuclei were localized at the rear/middle part of the nucleus.

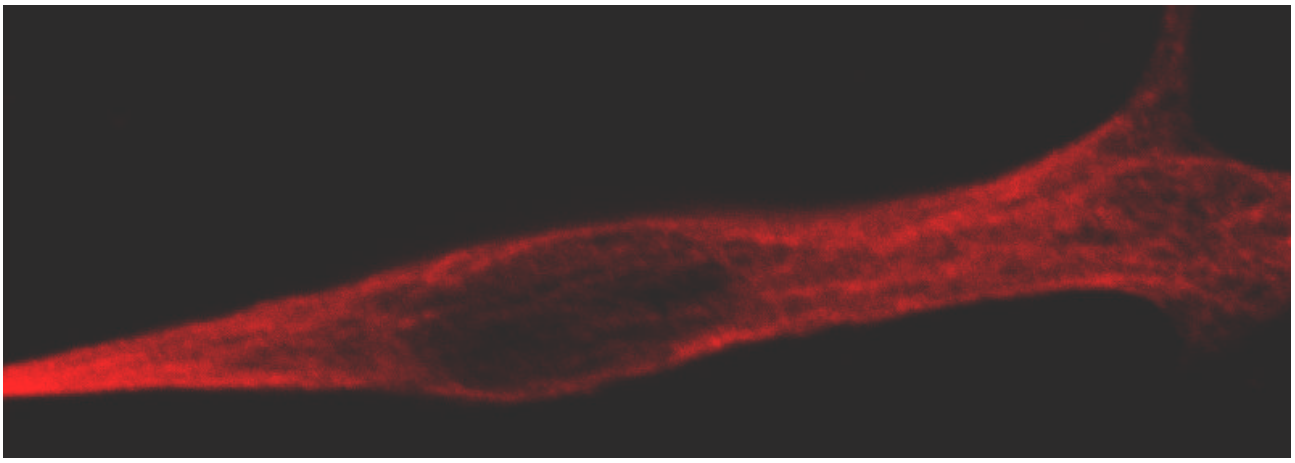

Figure 4.10: Microtubules imaged by confocal microscopy in an elongated C6 cell, which showed nuclear migration on a 20 μm wide stripe. Nucleus moved to the right, shape of the cell shows polarization with a narrow tail behind the nucleus and a wider leading edge. Distribution of MT-s is not apparently asymmetric, they mostly run parallel to the axis of the cell. In elongated cells high resolution imaging of MT-s was extremely difficult due to their closely packed structure.

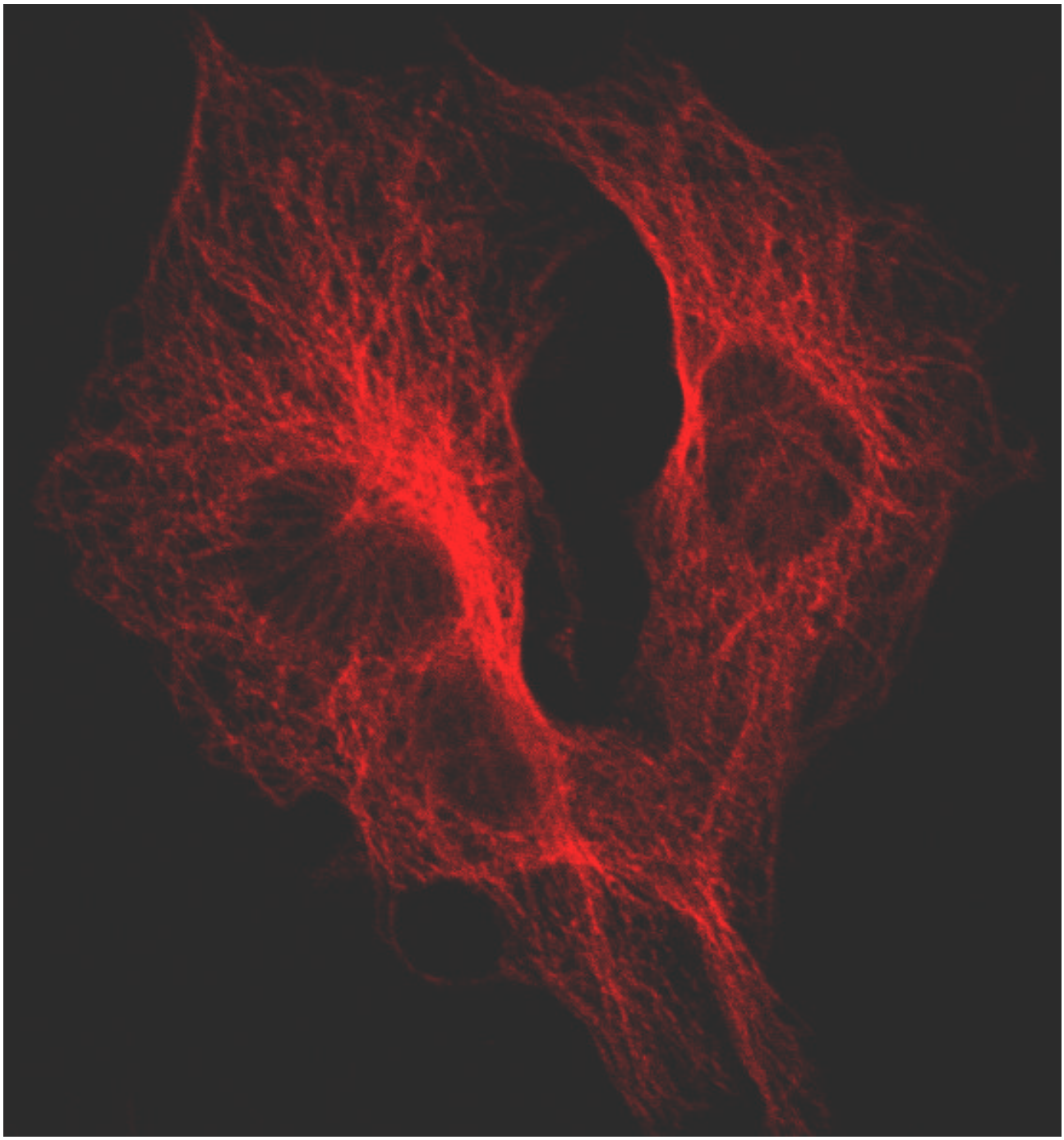

Figure 4.11: Fluorescent image of MT-s in cells from the same sample indicating that the same immuno-labeling procedure and imaging conditions give appropriate resolution in case of flattened cells.

Drug	Average nuclear velocity before the addition of the drug [μm/h]	Average nuclear velocity after the addition of the drug [μm/h]	Number of cells
no drug	29 ± 13		32
20 nM vinblastine	34 ± 0.4	3 ± 0.3	2
30 nM taxol	25 ± 11	8 ± 2	5
200 nM cytochalasin	13 ± 4	10 ± 5	4
1 μM (10 μM) ML-7	17 ± 7	19 ± 5 (28)	5 (1)
100 μM AMP-PNP	31 ± 10	34 ± 8	6
5 μM vanadate	30 ± 9	31 ± 11	4

Table 4.2: Effect of cytoskeleton affecting drugs on nuclear migration in C6 cells. We calculated the average velocity of each migrating nucleus, and then the mean value of these figures presented in the table with standard deviation after the $\pm$ symbol. MT disrupting vinblastine and MT stabilizing taxol had robust inhibitory effect on nuclear migration. F-actin disrupting cytochalasin D had slight impact at 200 nM. Kinesin inhibitor AMP-PNP and dynein inhibitor vanadate did not influence nuclear motility. Myosin-II inhibitor ML-7 did not change nuclear motility at 1 μM, and enhanced it at 10 μM.

reaches the end of the elongated cell and starts backward.

In the elongated C6 cells we observed that the migrating nucleus did not rotate, its orientation stayed fix during the turn back at the end of the cell, too. In flattened C6 cells we found that the nucleus could rotate, which is consistent with former studies indicating nuclear rotation to be general in several cell types [5]. Rotation of the nucleus was determined by tracking nucleoli that appear as dark dots in phase contrast images.

Chapter 5

Discussion

Using different techniques we succeeded to probe both cellular fluctuation on the nanometer scale and organized intracellular dynamics of the nucleus driven by an intriguing molecular mechanism.

5.1 Nanometer scale cellular fluctuations

Analysis of height fluctuations acquired at different locations on the cell allowed us to monitor the motility of cellular components sensitively. Both actin-myosin based contractions and actin polymerization-based filopodial and lamellipodial protrusions can be examined by this method. We found a correlation between the characteristics of vertical fluctuation and organized lateral locomotion.

We explain the observed 5 Hz pulsation of a cell with the periodic contractions of stress fibres. This type of oscillation cannot be easily identified by other techniques due to its low amplitude. Although the frequency of mechanical pulsation of cardiomyocytes is in the same frequency range ($\sim$1.25 Hz), its amplitude is 2 orders of magnitude higher [26]. Spontaneous oscillatory contractions of muscle fibers with a period of a few seconds are widely known for several years (e.g. [79]). Theoretical models can explain spontaneous oscillation under certain conditions [41]).

Slow pulsation of non-muscle cells has been observed in some cases. Microtubule depolymerization can induce rhythmic actomyosin-based contractility with a period of $\sim$50 s in fibroblasts [61] and oscillatory activity in the cortical microfilament system of lymphoblasts [13]. Shape oscillations of leukocytes driven by cyclic actin polymerization has been studied by several groups [29]. Period of this process is about $\sim$8 s.

Cortical tension of non-muscle cells generated by myosin-II can drive a change of shape [59]. Myosin molecules cycle about 5 times in a second in muscle [2]. Based on the above mentioned facts, we think that a synchronized behavior of myosin molecules in stress fibres may cause the observed pulsation. Myosin synchronization has been theoretically predicted close to the isometric

condition in highly organized actin structures [28, 27]. Further experiments are needed to elucidate the background of this phenomenon. Using drugs affecting a specific system of the cytoskeleton will help to distinguish their roles in the nanometer scale fluctuations of cells.

5.2 Nuclear motility in elongated cells

We found that the nucleus is motile in a high percentage of elongated cultured cells on the time scale of hours. Use of narrow (20 μm) protein/cell adhesive stripes separated by non-adhesive ones on plastic or glass surface was proved to be an adequate technique to control the cell shape, and force cells to acquire highly elongated form.

Cellular locomotion was inhibited on the narrow stripes. This fact helped us to study the motion of the nuclei clearly dissected from the locomotion of cells. We argue that cells can hardly migrate on the narrow stripes since the formation of normal lamellipodium at the edge of the cell is impossible: the typically wide leading edge cannot be developed.

Periodic (auto-reverse) nuclear migration is frequent in C6 glioma cells and primary mouse fibroblasts, and less frequent in 3T3 mouse fibroblasts. The nucleus of U87 human glioma cells is much less motile, which is attributed to their less elongated shape even on the narrow cell adhesive stripes. Period of periodic nuclear motility in C6 cells is $\sim$5 h, which is not in the range of their cell cycle being approximately 1 day. It means that probably there is no direct relationship between cell cycle and periodic nuclear migration. In case of primary mouse fibroblasts the average period is approximately 2 hours. Average velocity of periodic nuclear migration is similar in both cell types, i.e., the amplitude of nuclear migration is lower in fibroblasts. Time-lapse images show that the nucleus usually turns back before reaching the end of fibroblast cells; this results in lower amplitude and higher frequency.

F-actin disruption by cytochalasin D and myosin-II inhibition by the myosin light-chain kinase (MLCK) inhibitor ML-7 shows that the process is not sensitively actin- or myosin-dependent, which means that neither actin polymerization nor actomyosin based contraction drives the motion. Cytochalasin D slightly decreased the velocity of the nuclei. Nuclear migration was stopped by low concentrations of vinblastine or taxol. These are specific microtubule affecting drugs. Vinblastine cause the depolymerization of MT-s, taxol stabilizes them. Both drugs inhibit dynamic instability of MT-s. MT-dependent motors: kinesins and dyneins are known to be involved in the intracellular transport, and in nuclear positioning, too. We argue that they do not have central role in the nuclear migration studied by us. In case of a basically MT motor driven motility taxol would not block the motion since motors can walk along taxol stabilized MT-s. Inhibition of dynein by vanadate and kinesin by the ATP analogue AMP-PNP reinforced that cytoplasmic dyneins and kinesins were not crucial in nuclear migration.

Interaction between MT-s and F-actin is a complex and poorly understood field at this time. We think that it should be considered in nuclear migration. Both MT and actin systems are involved in cell polarization, which is thought to be a central problem in auto-reverse nuclear migration.

The centrosome in all the identified C6 cells with migrating nucleus was behind or beside the forward moving nucleus, never in front of it.

Previous experiments and theoretical considerations indicated that tubulin polymerization-depolymerization itself in the absence of MT motors is able to move the centrosome inside a chamber. Pushing force of a single polymerizing MT is in the range of pN-s. [38, 30, 25]. Nuclear migration in yeast cells [75, 24] also suggests that the polymerization force of MT-s can drive the nucleus attached to the microtubule organizing center. We propose that the nucleus is driven by the polimerization force of MT-s.

Motility of the nucleus is a slow, overdamped motion in a viscous medium. Although cell plasma is not a homogenous liquid (fibrous elements of the cytoskeleton have a significant impact on the drag sensed by the nucleus), it makes sense to consider an effective viscosity of the plasma [6, 15], which can vary but normally is in the range of 100 Pas. According to the Stokes Law we can estimate the force that moves the nucleus:

$$F = 6\pi\eta r v, \tag{5.1}$$

where F is the viscous force, η denotes the effective viscosity on the scale of the nucleus, r is the radius of the nucleus in the liquid, and v is the velocity of the nucleus that we measured. It gives a force in the 100 pN range, which means that $\sim$100 MT-s are pushing the nucleus forward. The result of the estimation is reasonable, since in a mitotic cell a few thousands of MT-s originate from the centrosome, a portion of them can take part in the pushing of the nucleus. During nuclear migration velocity of the nucleus is not constant but changes periodically, which may be caused by the change of the driving force or the effective viscosity.

Nuclear migration is driven and controlled by a complex system involving cytoskeletal elements and regulating proteins. On the basis of our experiments we conclude that the force, which drives nuclear migration in elongated cells, is MT-dependent, and it originates in MT polimerization. We think that the control of the process is related to cell polarization. Further experiments are in progress to clarify more details of this phenomenon.

In flattened C6 cells we found that the nucleus can rotate, which is consistent with former studies indicating nuclear rotation to be general in several cell types [5]. Nucleus in these cells is discus shaped, it can easily rotate in the plane of the cell. In the elongated C6 cells we observed that migrating nucleus did not rotate, its orientation stayed fix during the turn back at the end of the cell, too. A possible explanation of nuclear migration in elongated cells can be that the nucleus is unable to rotate inside the tight cell. Nuclei in these cells are squeezed: they have an oval shape. Nuclear

rotation in flattened cells might be driven by the force of polymerizing MT-s pushing the nucleus via the centrosome. In elongated cells similar pushing force of MT-s would result in the translation, i.e., migration of the nucleus. In this case, as the nucleus reaches the end of the elongated cell, the centrosome would slide on the nuclear membrane making a semicircle still being pushed by polymerizing MT-s (Fig. 5.1). (Similar motion of doubled centrosomes is well known at the beginning of mitosis.)

Turn back of the nucleus in primary mouse fibroblasts before reaching the end of the elongated cell might be caused by an easier sliding of the centrosome on the nuclear membrane. We think that in these cells the centrosome can be pushed to the other side of the nucleus during the migration far from the ends of the cell. Our observation that the centrosome can be at the front part of the nucleus in these cells during nuclear migration -in contrast with the behavior of C6 cells- is in agreement with this explanation.

Although this simple model fits with our results, further experiments should be carried out to clarify more details of the phenomenon in order to confirm the validity of our explanation.

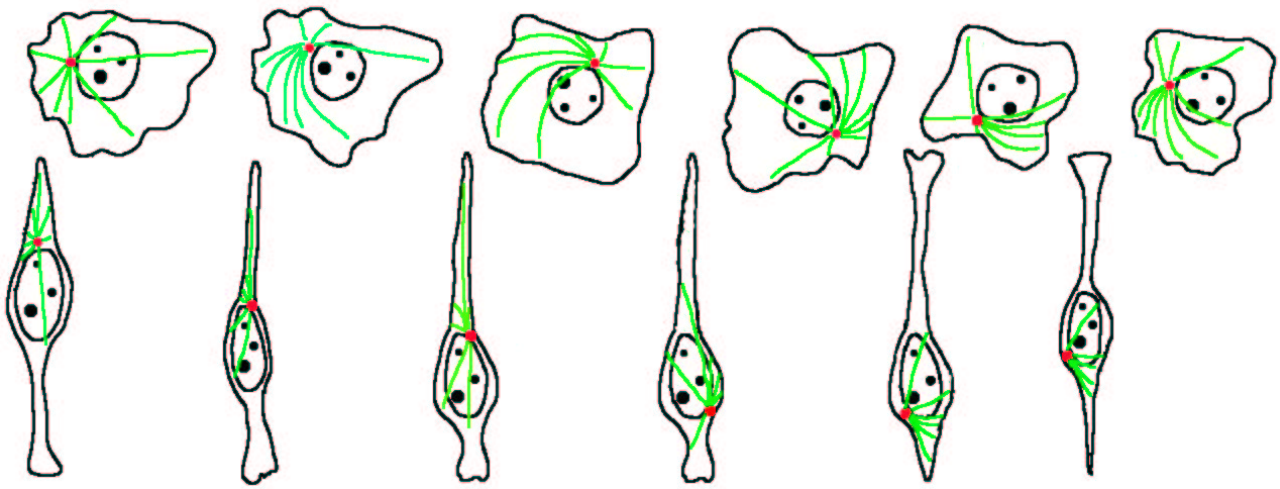

Figure 5.1: Schematic representation of a simple model that we propose to explain auto-reverse nuclear migration in elongated cells. Upper drawings show the rotation of the nucleus in a flattened cell. Microtubules (MT-s) are depicted in green, centrosome in red, nucleoli are represented by dark dots in the nucleus. Nucleus might be rotated by the pushing force of MT-s -showing dynamic instability- due to their partial alignment in the aster, which results in a torque. Partial alignment of MT-s can be maintained by the rotation itself. Such nuclear rotation in elongated cells (lower drawings) is inhibited: the squeezed oval nucleus is unable to rotate inside the tight cell. Pushing force of partially aligned MT-s in the aster with the centrosome in its center will rather translate the nucleus inside the cell. At the end of the cell the centrosome still being pushed by dynamic MT-s would slide on the nuclear membrane as long as the nucleus starts to migrate backward. Although the fact that polarization of the cell flips as the nucleus starts backward suggests a more complex mechanism, we think that this model will be useful, when establishing more sophisticated models on the basis of further experimental information.

Acknowledgments

I thank Noémi Rozlosnik for her extensive help in all fields of my graduate studies and experiments, especially in atomic force microscopy. I thank Tamás Vicsek for being very helpful in our co-operation, furthermore for his advisory efforts in the second part of my graduate years. I thank Dávid Selmeczi for his extraordinary helpfulness and invaluable work in our collaboration. I thank my further co-authors: Zsuzsanna Környei, Gábor Csúcs, András Czirók, Júlia Zách, Előd Méhes, Emília Madarász, Emma Hlavanda, Prof. János Kovács, Judit Ovádi -in published or not yet published cell biology related papers- for their work and kind co-operation. I thank Balázs Hegedűs for his help in cell biology, Zsófia Jurányi and Gergely Nagy for their work in data processing. I thank Miklós Csiszér, Ottó Haimann, Sándor Hopp, and Endre Berecz for their indispensable technical work in electronics, optics, and mechanics. I also thank my colleagues at the Department of Biological Physics for their kind helpfulness.

Bibliography

[1] V. C. Abraham, V. Krishnamurthi, D. L. Taylor, and F. Lanni. The actin-based nanomachine at the leading edge of migrating cells. *Biophys. J.*, 77(3):1721–32, 1999.

[2] B. Alberts, D. Bray, J. Lewis, M. Raff, K. Roberts, and J. D. Watson. *Molecular Biology of the Cell*. Garland Publishing, New York, 3rd edition, 1994.

[3] K. R. Ayscough. In vivo functions of actin-binding proteins. *Curr. Opinion Cell Biol.*, 10:102–111, 1998.

[4] J. Bain, H. McLauchlan, M. Elliott, and P. Cohen. The specificities of protein kinase inhibitors: an update. *Biochem J.*, 371:199–204, 2003.

[5] F. Bard, C. A. Bourgeois, D. Costagliola, and M. Bouteille. Rotation of the cell nucleus in living cells: a quantitative analysis. *Biol. Cell*, 54(2):135–42, 1985.

[6] A. R. Bausch, W. Moller, and E. Sackmann. Measurement of local viscoelasticity and forces in living cells by magnetic tweezers. *Biophys J.*, 76:573–79, 1999.

[7] P. Benda, J. Lightbody, G. Sato, L Levine, and W. Sweet. Differentiated rat glial cell strain in tissue culture. *Science*, 161:370–71, 1968.

[8] G. Binnig, C. F. Quate, and Ch. Geber. Atomic force microscope. *Phys. Rev. Lett.*, 56(9):930–33, 1986.

[9] G. Binnig and H. Rohrer. Scanning tunneling microscopy. *Helv. Phys. Acta*, 55:726, 1982.

[10] A. L. Bishop and A. Hall. Rho gtpases and their effector proteins. *Biochem. J.*, 348:241–55, 2000.

[11] M. V. Blagosklonny and T. Fojo. Molecular effects of paclitaxel: myths and reality (a critical review). *Int. J. Cancer*, 83:151–56, 1999.

[12] G. G. Borisy and T. M. Svitkina. Actin machinery: pushing the envelope. *Curr. Opin. Cell. Biol.*, 12(1):104–12, 2000.

[13] M. Bornens, M. Paintrand, and C. Celati. The cortical microfilament system of lymphoblasts displays a periodic oscillatory activity in the absence of microtubules: implications for cell polarity. *J. Cell. Biol.*, 109(3):1071–83, 1989.

[14] H. J. Butt, E. K. Wolff, S. A. Gould, B. Dixon Northern, C. M. Peterson, and P. K. Hansma. Imaging cells with the atomic force microscope. *J. Struct. Biol.*, 105:54–61, 1990.

[15] A. Caspi, R. Granek, and M. Elbaum. Diffusion and directed motion in cellular transport. *Phys. Rev. E*, 66:011916, 2002.

[16] H. Chen, B. W. Bernstein, and J. R. Bamburg. Regulating actin-filament dynamics in vivo. *TIBS*, 25:19–23, 2000.

[17] E. Chytilova, J. Macas, E. Sliwinska, S. M. Rafelski, G. M. Lambert, and D. W. Galbraith. Nuclear dynamics in arabidopsis thaliana. *Mol. Biol. Cell*, 11(8):2733–41, 2000.

[18] E. A. Cox, S. K. Sastry, and A. Huttenlocher. Integrin-mediated adhesion regulates cell polarity and membrane protrusion through the rho family of gtpases. *Mol. Biol. Cell*, 12:265–77, 2001.

[19] G. Csúcs, G. R. Michel, J. W. Lussi, M. Textor, and G. Danuser. Microcontact printing of novel co-polymers in combination with proteins for cell-biological applications. *Biomaterials*, 24(10):1713–20, 2003.

[20] A. Czirók, K. Schlett, E. Madarász, and T. Vicsek. Exponential distribution of locomotion activity in cell cultures. *Phys. Rev. Lett.*, 81(14):3038–41, 1998.

[21] B. A. Danowski, A. Khodjakov, and P. Wadsworth. Centrosome behavior in motile hgf-treated ptk(2) cells expressing gfp-gamma tubulin. *Cell. Motil. Cytoskeleton*, 50(2):59–68, 2001.

[22] G. Danuser and R. Oldenbourg. Probing f-actin flow by tracking shape fluctuations of radial bundles in lamellipodia of motile cells. *Biophys. J.*, 79(1):191–201, 2000.

[23] C. Lambert de Rouvroit and A. M. Goffinet. Neuronal migration. *Mech. Dev.*, 105:47–56, 2001.

[24] D-Q. Ding, Y. Chikashige, T. Haraguchi, and Y. Hiraoka. Oscillatory nuclear movement in fission yeast meiotic prophase is driven by astral microtubules, as revealed by continuous observation of chromosomes and microtubules in living cells. *J. Cell Sci.*, 111:701–712, 1998.

[25] M. Dogterom and B. Yurke. Microtubule dynamics and the positioning of microtubule organizing centers. *Phys. Rev. Lett.*, 81(2):485–88, 1998.

[26] J. Domke, W. J. Parak, M. George, H. E. Gaub, and M. Radmacher. Mapping the mechanical pulse of single cardiomyocytes with the atomic force microscope. *Eur. Biophys. J.*, 28:179–86, 1999.

[27] T. Duke. Cooperativity of myosin molecules through strain-dependent chemistry. *Philos. Trans. R. Soc. Lond. B Biol. Sci.*, 355(1396):529–38, 2000.

[28] T. A. J. Duke. Molecular model of muscle contraction. *PNAS*, 96:2770–75, 1999.

[29] M. U. Ehrengruber, D. A. Deranleau, and T. D. Coates. Shape oscillations of human neutrophil leukocytes: characterization and relationship to cell motility. *J. Exp. Biol.*, 199:741–47, 1996.

[30] C. Faivre-Moskalenko and M. Dogterom. Dynamics of microtubule asters in microfabricated chambers: The role of catastrophes. *PNAS*, 99:16788–19793, 2002.

[31] D. R. Friedlander, P. A. Brittis, T. Sakurai, B. Shif, W. Wirchansky, G. Fishell, and M. Grumet. Generation of a radial-like glial cell line. *J Neurobiol*, 37(2):291–304, 1998.

[32] I. S. Grigoriev, A. A. Chernobelskaya, and I. A. Vorobjev. Nocodazole, vinblastine and taxol at low concentrations affect fibroblast locomotion and saltatory movements of organelles. *Membr. Cell Biol.*, 13(1):23–48, 1999.

[33] H. Haga, M. Nagayama, K. Kawabata, E. Ito, T. Ushiki, and T. Sambongi. Time-lapse viscoelastic imaging of living fibroblasts using force modulation mode in afm. *J. Electron Microsc.*, 49(3):473–81, 2000.

[34] P. K. Hansma, J. P. Cleveland, M. Radmacher, D.A. Walters, P. Hillner, M. Bezanilla, M. Fritz, D. Vie, H.G. Hansma, C.B. Prater, J. Massie, L. Fukunaga, J. Gurley, and V. Elings. Tapping mode atomic force microscopy in liquids. *Applied Physics Letters*, 64(13):1738/40, 1994.

[35] B. Hegedűs, A. Czirók, I. Fazekas, T. Bábel, E. Madarász, and T. Vicsek. Locomotion and proliferation of glioblastoma cells in vitro: statistical evaluation of videomicroscopic observations. *J Neurosurg*, 92(3):428–34, 2000.

[36] E. Henderson, P. G. Haydon, and D. S. Sakaguchi. Actin filament dynamics in living glial cells imaged by atomic force microscopy. *Science*, 257:1944–46, 1992.

[37] U. G. Hofmann, C. Rotsch, W. J. Parak, and M. Radmacher. Investigating the cytoskeleton of chicken cardiocytes with the atomic force microscope. *J. Struct. Biol.*, 119(2):84–91, 1997.

[38] T. E. Holly, M. Dogterom, B. Yurke, and S. Leibler. Assembly and positioning of microtubule asters in microfabricated chambers. *PNAS*, 96:6228–31, 1997.

[39] A. Holzinger and U. Lutz-Meindl. Kinesin-like proteins are involved in postmitotic nuclear migration of the unicellular green alga micrasterias denticulata. *Cell Biol. Int.*, 26(8):689–97, 2002.

[40] K. Homma, M. Yoshimura, J. Saito, R. Ikebe, and M. Ikebe. The core of the motor domain determines the direction of myosin movement. *Nature*, 412(6849):831–41, 2001.

[41] F. Jülicher, A. Ajdari, and J. Prost. Modeling molecular motors. *Rev. Mod. Phys.*, 69(4):1269–81, 1997.

[42] K. Kaibuchi, S. Kuroda, and M. Amano. Regulation of the cytoskeleton and cell adhesion by the rho family gtpases inmammalian cells. *Annu. Rev. Biochem.*, 68:459–486, 1999.

[43] J. Klominek, K-G. Sundqvist, and K-H. Robért. Nucleokinesis: Distinct pattern of cell translocation in response to an autocrine motility factor-like substance or fibronectin. *PNAS*, 88:3902–06, 1991.

[44] Zs. Környei, A Czirók, T. Vicsek, and E. Madarász. Proliferative and migratory responses of astrocytes to in vitro injury. *J. Neurosci Res.*, 61:421–29, 2000.

[45] M. Lekka, P. Laidler, D. Gil, J. Lekki, Z. Stachura, and A. Z. Hrynkiewicz. Elasticity of normal and cancerous human bladder cells studied by scanning force microscopy. *Eur. Biophys. J.*, 28:312–16, 1999.

[46] R. Lévy and M. Maaloum. Measuring the spring constant of atomic force microscope cantilevers: thermal fluctuations and other methods. *Nanotechnology*, 13:33–37, 2002.

[47] L. M. Machesky and A. Hall. Role of actin polymerization and adhesion to extracellular matrix in rac- and rho-induced cytoskeletal reorganization. *J. Cell Biology*, 138:913–26, 1997.

[48] S. N. Magonov and M-H Whangbo. *Surface analysis with STM and AFM*. VCH, 1996.

[49] L. Mahadevan and P. Matsudaira. Motility powered by supramolecular springs and ratchets. *Science*, 288:95–99, 2000.

[50] R. Michel, J. W. Lussi, G. Csucs, I. Reviakine, G. Danuser, B. Ketterer, J. A. Hubbell, M. Textor, and N. D. Spencer. Selective molecular assembly patterning: A new approach to micro- and nanochemical patterning of surfaces for biological applications. *Langmuir*, 18:3281–87, 2002.

[51] A. Mogilner and G. Oster. Cell motility driven by actin polymerization. *Biophys. J.*, 71(6):3030–45, 1996.

[52] N. R. Morris. Nuclear migration: from fungi to the mammalian brain. *J. Cell Biol.*, 148(6):1097–1101, 2000.

[53] N. R. Morris. Nuclear positioning: the means is at the ends. *Curr. Opin. Cell. Biol.*, 15(1):54–59, 2003.

[54] A. Murciano, J. Zamora, J. Lopez-Sanchez, and J. M. Frade. Interkinetic nuclear movement may provide spatial clues to the regulation of neurogenesis. *Mol. and Cell. Neuroscience*, 21:285–300, 2002.

[55] J. W. Murray, E. Bananis, and A. W. Wolkoff. Reconstitution of atp-dependent movement of endocytic vesicles along microtubules in vitro: an oscillatory bidirectional process. *Mol. Biol. Cell*, 11(2):419–33, 2000.

[56] B. Nadarajah and J. G. Parnavelas. Modes of neuronal migration in the developing cerebral cortex. *Nature Reviews Neuroscience*, 3:423–32, 2002.

[57] M. Y. Niu, J. C. Mills, and V. T. Nachmias. Development of polarity in human erythroleukemia cells: roles of membrane ruffling and the centrosome. *Cell. Motil. Cytoskeleton*, 36(3):203–15, 1997.

[58] V. Parpura, P. G. Haydon, and E. Henderson. Three-dimensional imaging of living neurons and glia with the atomic force microscope. *J. Cell Sci.*, 104:427–32, 1993.

[59] C. Pasternak, J. A. Spudich, and E. L. Elson. Capping of surface receptors and concomitant cortical tension are generated by conventional myosin. *Nature*, 341:549–51, 1989.

[60] Ch. S. Peskin, G. M. Odell, and G. F. Oster. Cellular motions and thermal fluctuations: the brownian ratchet. *Biophys. J.*, 65:316–24, 1993.

[61] O. J. Pletjushkina, Z. Rajfur, P. Pomorski, T. N. Oliver, J. M. Vasiliev, and K. A. Jacobson. Induction of cortical oscillations in spreading cells by depolymerization of microtubules. *Cell. Motil. Cytoskeleton*, 48(4):235–44, 2001.

[62] J. Ponten and E. H. Macintyre. Long term culture of normal and neoplastic human glia. *Acta. Pathol. Microbiol. Scand.*, 74(4):465–86, 1968.

[63] S. Reinsch and P. Gönczy. Mechanisms of nuclear positioning. *J. Cell Sci.*, 111:2283–95, 1998.

[64] C. Rotsch and M. Radmacher. Drug-induced changes of cytoskeletal structure and mechanics in fibroblasts: an atomic force microscopy study. *Biophys. J.*, 78(1):520–35, 2000.

[65] Ch. Rotsch, K. Jacobson, and M. Radmacher. Dimensional and mechanical dynamics of active and stable edges in motile fibroblasts investigated by using atomic force microscopy. *PNAS*, 96:921–26, 1999.

[66] S. W. Schneider, K. C. Sritharan, J. P. Geibel, H. Oberleithner, and B. P. Jena. Surface dynamics in living acinar cells imaged by atomic force microscopy: identification of plasma membrane structures involved in exocytosis. *PNAS*, 94:316–21, 1997.

[67] C. A. Shönenberger and J. H. Hoh. Slow cellular dynamics in mdck and r5 cells monitored by time-lapse atomic force microscopy. *Biophys. J.*, 67(2):929–36, 1994.

[68] L. L. Soethout, H. van Kempen, and G. F. A. van de Walle. *Scanning Tunneling Microscopy: A mature surface-science technique in advances in electronics and electron physics*. Academic Press, 1990.

[69] O. Speck, S. C. Hughes, N. K. Noren, R. M. Kulikauskas, and R. G. Fehon. Moesin functions antagonistically to the rho pathway to maintain epithelial integrity. *Nature*, 421:83–87, 2003.

[70] T. M. Svitkina, A. B. Verkovsky, K. M. McQuade, and G. M. Borisy. Analysis of the actin-myosin ii system in fish epidermal keratocytes: Mechanism of cell body translocation. *J. Cell Biology*, 139(2):397–415, 1997.

[71] B. Szabó, Zs. Környei, G. Csúcs, A. Czirók, D. Selmeczi, J. Zách, and T. Vicsek. Auto-reverse nuclear migration in mammalian cells can be induced by enforcing bipolarity in vitro, to be published.

[72] B. Szabó, D. Selmeczi, Zs. Környei, E. Madarász, and N. Rozlosnik. Atomic force microscopy of height fluctuations of fibroblast cells. *Phys. Rev. E*, 65:041910, 2002.

[73] T. Wakatsuki T, B. Schwab, N. C. Thompson, and E. L. Elson. Effects of cytochalasin d and latrunculin b on mechanical properties of cells. *J. Cell Sci.*, 14(5):1025–36, 2001.

[74] G. J. Todaro and H. Green. *J. Cell Biol.*, 17:299–313, 1963.

[75] P. T. Tran, L. Marsh, V. Doye, S. Inoue, and F. Chang. A mechanism for nuclear positioning in fission yeast based on microtubule pushing. *J. Cell Biol.*, 153(2):397–411, 2001.

[76] R. D. Vale and R. J. Fletterick. The design plan of kinesin motors. *Annu Rev Cell Dev Biol*, 13:745–77, 1997.

[77] F. A. J. M. van de Klundert, J. M. H. Raats, and H. Blomendal. Intermediate filaments: regulation of gene expression and assembly. *Eur. J. Biochemistry*, 214:351–66, 1993.

[78] T. Vicsek. *Fluctuations and scaling in biology*. Oxford University Press, Oxford, 2001.

[79] K. Yasuda, Y. Shindo, and S. Ishiwata. Synchronous behavior of spontaneous oscillations of sarcomeres in skeletal myofibrils under isotonic conditions. *Biophys. J.*, 70(4):1823–29, 1996.

[80] A. M. Yvon, J. W. Walker, B. Danowski, C. Fagerstrom, A. Khodjakov, and P. Wadsworth. Centrosome reorientation in wound-edge cells is cell type specific. *Mol. Biol. Cell.*, 13(6):1871–80, 2002.

[81] J. Zlatanova, S. M. Lindsay, and S. H. Leuba. Single molecule force spectroscopy in biology using the atomic force microscope. *Prog Biophys Mol Biol*, 74:37–61, 2000.

Summary

Motion of animals is a beautiful and complex feature of life, which can be incredibly organized. There is a natural scientific need to understand biological motion. In our cells on the level of molecular motors motion is rather stochastic dominated by fluctuations. Cellular motility is between the organized macroscopic behavior of animals and the random motion of microscopic molecules: cells show both stochastic and highly controlled motility. The link between random and organized motion is not straightforward and its many aspects are unclear.

We attempted to investigate cellular motility down to the nanometers to provide information of the fluctuations of cells. Fluctuation driven stochastic motion of the molecules transforms to organized/controlled motion in the range of micrometers. Studying an intriguing example of intracellular motion -nuclear migration- we tried to give a better understanding of a type of controlled biological motility, which still shows stochastic features, and in this sence, it is on a mesoscopic scale.

We used cultured animal cells in our experiments. Atomic force microscope (AFM) was applied to investigate the dynamics of cells at high resolution. In our nuclear migration studies the primary tool was automated time lapse phase contrast microscopy. A micropatterned protein surfaces was used to control the cell shape. We employed specific drugs -inhibitors- to affect some cytoskeletal elements. Immunocytochemistry in correlation with previous time lapse microscopy of cells was applied to acquire information on the molecular background of the motion.

We showed that atomic force microscopy can be successfully utilized for measuring the nanometer scale fluctuations of cells in culture, and we found that the statistical analysis of these fluctuations provides relevant biological information. Intracellular dynamics can be probed by this method, as well. The level of height fluctuations is higher at the leading edge than at the rather quiescent, stable regions of the cells due to actin polymerization. We observed fast periodic motility on a cell, which was attributed to a theoretically predicted effect: synchronization of myosin molecules in muscle-like structures (stress fibers) close to the isometric condition.

We demonstrated that nuclear motility can be investigated under precisely controlled conditions using micropatterned surfaces and time lapse microscopy, and found that nuclear migration in some cell lines is strongly dependent on the geometry of cells; further factors have only moderate effect on the phenomenon. Nuclear migration takes place in elongated cells, in case of other cell shapes the nu-

cleus does not show long term migration. We observed that the nucleus can turn back in the elongated cell almost immediately after reaching its end. This auto-reverse phenomenon is frequent in a glioma cell line (C6) and primary mouse fibroblasts, and less frequent in some other investigated cell types. Using specific drugs we concluded that nuclear migration (a general effect in cell biology) is driven by microtubule polymerization. In C6 cells the centrosome stays at the rear part of the migrating nucleus. When the nucleus turns back, the centrosome is pushed to the other side of it, maintaining the lagging position of the centrosome. We propose a simple model to explain the phenomenon of auto-reverse nuclear migration. Further experiments should be carried out to confirm the validity of this model.

Összefogló

This is the 2nd page of the osszefoglalo.